

## Dynamics of Barotropic Storm Tracks

KYLE L. SWANSON AND PAUL J. KUSHNER

*Program in Atmospheric and Oceanic Sciences, Princeton University, Princeton, New Jersey*

ISAAC M. HELD

*Geophysical Fluid Dynamics Laboratory/NOAA, Princeton, New Jersey*

(Manuscript received 10 June 1996, in final form 29 August 1996)

### ABSTRACT

Longitudinal variations in the upper-tropospheric time-mean flow strongly modulate the structure and amplitude of upper-tropospheric eddies. This barotropic modulation is studied using simple models of wave propagation through zonally varying basic states that consist of contours separating regions of uniform barotropic potential vorticity. Such basic states represent in a simple manner the potential vorticity distribution in the upper troposphere. Predictions of the effect of basic-state zonal variations on the amplitude and spatial structure of eddies and their associated particle displacements are made using conservation of wave action or, equivalently, the linearized “pseudoenergy” wave activity. The predictions are confirmed using WKB theory and linear numerical calculations. The interaction of finite-amplitude disturbances with the basic flow is also analyzed numerically using nonlinear contour-dynamical simulations. It is found that breaking nonlinear contour waves undergo irreversible amplitude attenuation, scale lengthening, and frequency lowering upon passing through a region of weak basic-state flow.

### 1. Introduction

The longitudinal structure of the midlatitude storm tracks is determined not only by zonal variations in the lower-tropospheric baroclinicity (Hoskins and Valdes 1990), but also by zonal variations in the barotropic mean flow that control the reversible and irreversible deformation of upper-level disturbances. For example, eddies propagating into a split jet stream typically undergo zonal compression and meridional extension, as well as simultaneous modulation of their middle- and upper-tropospheric geopotential amplitude (Mullen 1987; Dole 1986; Lau 1988; Nakamura and Wallace 1993). However, the quantitative relationship between these eddy structural changes and the zonal variations of the underlying time-mean flow is not well understood. Understanding this relationship is a necessary first step in constructing a theory of the time-mean effects of eddies upon the mean flow.

Even for the relatively simple case of small-amplitude eddies undergoing reversible deformation, it is not clear how strongly eddies are modulated by a zonally varying flow. Lee (1995) makes the point that certain measures

of eddy variance may indicate strong modulation of variance while others may not. In her linearized model, the eddy enstrophy is approximately uniform zonally, but the geopotential variance and eddy energy are not and decrease sharply where the zonal flow is locally weak.

We have, therefore, been motivated to examine more closely barotropic wave propagation on zonally varying basic flows using highly simplified models. The models we consider consist of one or two discontinuities in the barotropic potential vorticity (PV), or “contours,” separating regions of homogeneous PV. This modeling approach is motivated not only by its analytical and numerical accessibility, but also by the observation that PV in the upper troposphere is characterized by local regions of sharp gradients (e.g., Hoskins et al. 1985). Additionally, such models provide instructive examples of how wave propagation behavior changes when the eddy amplitudes are sufficiently large to cause irreversible wave breaking.

Consider the simplest case of a single PV contour located at  $y = 0$  on an infinite  $f$  plane, separating a region of PV of value  $Q$  to the south from a region of PV of value  $Q + \Delta$  to the north of the contour, along with the associated zonal flow  $U(y)$ . The dispersion relation for waves on the contour (see section 3a) is

$$\omega = U_0 k - \Delta/2, \quad (1.1)$$

---

*Corresponding author address:* Dr. Paul J. Kushner, Program in Atmospheric and Oceanic Sciences, Princeton University, Princeton, NJ 08544.  
E-mail: pjk@gfdl.gov

where  $k$  is the zonal wavenumber and  $U_0 = U|_{y=0}$ . As for the classical  $\beta$ -plane Rossby wave (Pedlosky 1987, chapter 3), the phase speed of these waves for positive northward PV jump  $\Delta$  is always slower than the flow speed on the contour and approaches the value of the flow speed on the contour in the short-wave limit. Of course, there are important differences: unlike the  $\beta$ -plane Rossby waves, the group velocity of these waves has no meridional component and the zonal component equals  $U_0$ , independent of  $k$ .

Wave propagation on PV contours is considerably simpler than propagation on continuous PV distributions because waves on PV contours are edge waves that remain trapped in the vicinity of the contour. In the simple one-contour example just introduced, normal-mode solutions have the form  $\psi \propto e^{i(kx - \omega t)} e^{-k|y|}$ , that is, trapped waves with a meridional decay scale equal to their zonal scale. Classical Rossby waves, by contrast, are not meridionally localized. Waves on PV contours cannot radiate meridionally because of the absence of any PV gradient in the surrounding fluid.

The confinement of the eddies close to the PV contours circumvents a significant difficulty encountered in the analysis of small-amplitude wave propagation on jets with continuously varying cross-stream PV (e.g., Hoskins and Ambrizzi 1993). Typically, synoptic-scale eastward propagating waves on a jet have critical lines (where the phase speed of the waves equals the local flow speed) on the jet flanks. Irreversible breaking and mixing near the critical lines creates a “lossy” wave guide even for small-amplitude waves, as in Dickinson’s (1968) model of vertically propagating waves in the stratosphere, unless the PV is sufficiently mixed in the vicinity of the critical lines, as indicated by nonlinear critical layer theory (Warn and Warn 1978; Killworth and McIntyre 1985). Contour models avoid these complications for small-amplitude waves; heuristically, one can think of the PV mixing on either side of the jet as having proceeded to completion due to prior eddy effects, leaving the contour as a “loss-free” wave guide. Given the relative simplicity of the linear contour problem, nonlinearities can be introduced in a controlled manner to study how the behavior of the system changes when the eddy amplitudes become large enough to cause irreversible wave breaking.

In this study, we examine the effect of zonal variations in the basic flow on contour wave structure for both small-amplitude and finite-amplitude waves. We use a variety of approaches in the analysis, including conservation of wave action (Whitham 1965; Bretherton and Garrett 1968), and the closely related conservation of wave “pseudoenergy” (Arnol’d 1966; McIntyre and Shepherd 1987), WKB theory, and linear and nonlinear numerical simulations. Section 2 outlines the dynamical equations and conservation properties for general piecewise-constant barotropic PV distributions. Section 3 explores the simplest model “storm track,” namely the contour model introduced above, but with a zonally

varying basic flow on the contour. The predictions of the linear theory are verified numerically, and the nature of the nonlinear wave breaking that occurs for finite-amplitude wave packets is examined. Section 4 extends this inquiry to storm tracks with two PV contours, and the results are discussed in section 5. To simplify the presentation, details of the derivations of the linearized perturbation equation and of pseudoenergy conservation, and the WKB analysis for the one-contour model are included in the appendixes.

## 2. Wave dynamics on contours

### a. Equations of motion

Consider barotropic dynamics on an  $f$  plane with topography forcing a zonally varying yet steady basic flow. The basic flow streamfunction  $\Psi$  and barotropic PV  $Q$  are related by

$$Q = f_0 + \nabla^2 \Psi + f_0 \frac{H(x, y)}{H_{\text{ref}}}, \quad (2.1)$$

where  $H(x, y)$  is the topography,  $H_{\text{ref}}$  the reference depth of the fluid, and  $f_0$  the Coriolis parameter. The equation of motion for the steady basic flow is

$$\partial_{xy}(\Psi, Q) = 0, \quad (2.2)$$

where  $\partial_{xy}(f, g) \equiv \partial_x f \partial_y g - \partial_y f \partial_x g$  is the two-dimensional Jacobian. Perturbations to this flow evolve according to

$$\frac{\partial q}{\partial t} + \partial_{xy}(\Psi, q) + \partial_{xy}(\psi, Q) + \partial_{xy}(\psi, q) = 0, \quad (2.3)$$

where  $\psi$  and  $q \equiv \nabla^2 \psi$  are the disturbance streamfunction and PV, respectively.

The basic-state PV distribution is assumed to consist of  $N + 1$  regions of constant PV  $Q_j$  separated by  $N$  PV jumps:

$$\Delta_j \equiv Q_{j+1} - Q_j \text{ at } y = y_j(x), \quad j = 1, \dots, N, \quad (2.4)$$

located at the contours  $y_j(x)$ , where we assume that each  $y_j$  is single valued in  $x$  for simplicity. These PV jumps are associated with jumps in the shear of the along-contour wind. Because the basic-state flow is steady, the contours are also streamlines; typical flow scenarios for  $N = 1$  and  $N = 2$  and  $\delta$  function topography are schematically illustrated in Fig. 1.

Away from the contours, the PV is constant and the disturbance PV vanishes; that is,

$$\nabla^2 \psi = 0, \text{ away from contours.} \quad (2.5)$$

In appendix A, the dynamical equation for linear perturbations,

$$\frac{\partial}{\partial t}([\partial_n \psi]_j) + \frac{\partial}{\partial s}(U_j[\partial_n \psi]_j) + \Delta_j \partial_s \psi_j = 0 \text{ at contour } j, \quad (2.6)$$

is derived using (2.3) and the delta-function character

of the PV gradients in the basic-state flow. In (2.6),  $n$  and  $s$  are the local coordinates normal and tangential to contour  $j$ , respectively;  $U_j$  is the velocity on and tangential to contour  $j$ ; and the notation  $[\xi] = \lim_{\epsilon \rightarrow 0} (\xi|_{n=+\epsilon} - \xi|_{n=-\epsilon})$  indicates a jump in the quantity  $\xi$  across the contour. Additional boundary conditions on the perturbation streamfunction  $\psi$  are that it must be continuous everywhere and must vanish for  $|y| \rightarrow \infty$ .

An eddy field of great importance is  $\eta$ , the Lagrangian displacement of the contour normal to its basic-state position. It is shown in appendix A that (2.6) leads to the following relation between  $\psi$ , the disturbance streamfunction, and  $\eta$  for small amplitude displacements:

$$\eta_j = -\frac{[\partial_n \psi]_j}{\Delta_j}. \tag{2.7}$$

*b. Conserved quantities*

One goal of this work is to use quantities that are conserved by eddies propagating through zonally varying contour distributions to quantify the effect of zonal variations on eddy amplitudes and particle displacements. One such conserved disturbance quantity is the pseudoenergy wave activity (Arnol'd 1966; McIntyre and Shepherd 1987), a quantity defined for finite-amplitude disturbances to steady basic states. The pseudoenergy is an exact invariant of the nonlinear barotropic PV equation (2.3). In appendix B, finite- and small-amplitude expressions for the pseudoenergy  $\mathcal{A}$  for piecewise-constant PV distributions are derived. The pseudoenergy satisfies

$$\frac{d\mathcal{A}}{dt} = 0, \quad \text{where } \mathcal{A} = \mathcal{E} + \mathcal{B}. \tag{2.8}$$

In (2.8),  $\mathcal{E}$  is the domain-integrated disturbance energy,

$$\mathcal{E} = \int_{\text{domain}} \frac{1}{2}(u^2 + v^2) dx dy, \tag{2.9}$$

where  $u = -\partial_y \psi$  and  $v = \partial_x \psi$ , and  $\mathcal{B}$  is the domain integral of the ‘‘generalized enstrophy’’ density (McIntyre and Shepherd 1987).

For small-amplitude disturbances to a contour distribution, both the energy and the generalized enstrophy may be written in a form that involves only quantities evaluated on the contour:

$$\mathcal{E} \approx \sum_{j=1}^N \int_{y_j} \frac{1}{2} \Delta_j \psi_j \eta_j ds = \sum_{j=1}^N \int_{y_j} E_{c_j} ds,$$

and

$$\mathcal{B} \approx \sum_{j=1}^N \int_{y_j} -\frac{1}{2} U_j \Delta_j \eta_j^2 ds, \tag{2.10}$$

where  $\psi_j$  is the disturbance streamfunction on the contour,  $U_j$  is the velocity on and tangential to the contour,

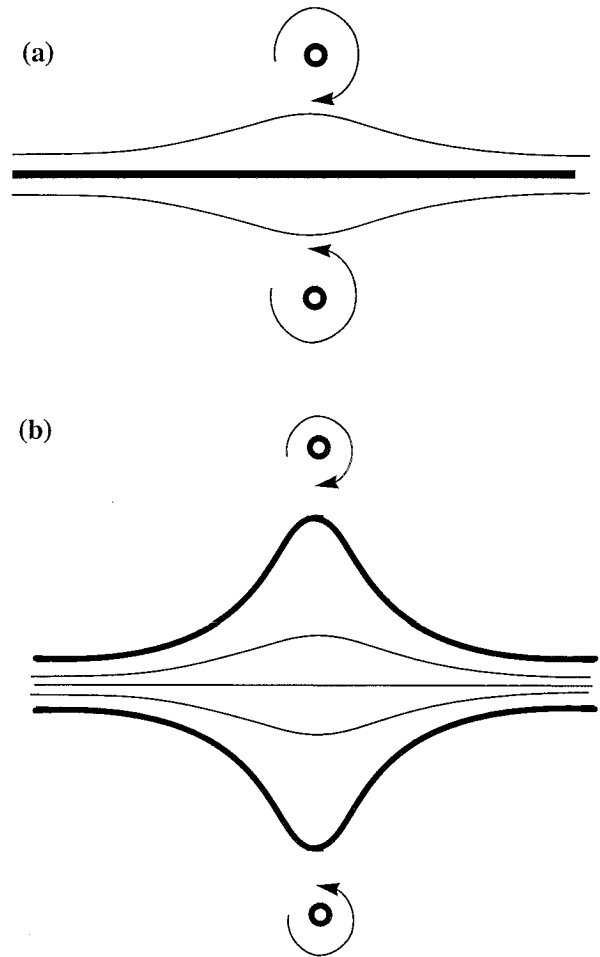


FIG. 1. Schematic representation of one- and two-contour PV distributions. Thick contours represent PV jumps, thin contours represent typical streamlines, and small circles represent topography with associated forcing.

and  $E_{c_j}$  is the energy density associated with the  $j$ th contour.

A related conserved disturbance quantity is the wave action (Whitham 1965; Bretherton and Garrett 1968; see the review by Grimshaw 1984), which is conserved for eddies propagating on slowly varying basic states. From general principles (Andrews and McIntyre 1978), pseudoenergy conservation reduces to wave action conservation for linear disturbances on slowly varying basic states. Consider wavelike disturbances with local wavenumber  $k$  (associated with the  $s$  coordinate) and frequency  $\omega$ , propagating through a basic state that varies on some slow spatial scale  $S = \epsilon s$  along the contour, where  $\epsilon \ll 1$ . To leading order in  $\epsilon$ , the linearized equation of motion (2.6) on the  $j$ th contour can be written

$$\psi_j - U_j \eta_j = -\omega \eta_j / k, \tag{2.11}$$

where we have used (2.7). Equation (2.11) can also be written

$$\eta_j = -k \psi_j / \hat{\omega}_j, \tag{2.12}$$

where  $\hat{\omega}_j \equiv \omega - U_j k$  is the local intrinsic frequency on the  $j$ th contour (i.e., the frequency measured in a reference frame moving with the local basic flow on the contour). Substituting (2.12) into (2.10) and (2.8), and taking a phase average, we find

$$\frac{d}{dt} \sum_{j=1}^N \int_{y_j} \frac{\omega}{\hat{\omega}_j} \left\langle \frac{1}{2} \Delta_j \psi_j \eta_j \right\rangle ds = \frac{d}{dt} \sum_{j=1}^N \int_{y_j} \omega \frac{\langle E_{cj} \rangle}{\hat{\omega}_j} ds = 0, \tag{2.13}$$

where the angled brackets denote phase averaging. For a time-independent basic flow, under the WKB approximation the frequency  $\omega$  is constant during disturbance propagation. We can therefore identify the quantity

$$W_j \equiv \frac{\langle E_{cj} \rangle}{\hat{\omega}_j} \tag{2.14}$$

as the wave action associated with the  $j$ th contour, whose sum over all contours  $\mathcal{W} = \sum_{j=1}^N W_j$  is conserved:

$$\frac{d}{dt} \int \mathcal{W} ds = 0. \tag{2.15}$$

The local conservation law for the wave action is

$$\frac{\partial \mathcal{W}}{\partial T} + \frac{\partial}{\partial S} (c_g \mathcal{W}) = 0, \tag{2.16}$$

where  $c_g = \partial \omega / \partial k$  is the local group velocity and  $T = \epsilon t$ . For a steady wave train, (2.16) implies that  $c_g \mathcal{W}$  is independent of  $s$ . Manipulation of (2.16) yields

$$\frac{1}{c_g \mathcal{W}} \frac{d_g}{dT} (c_g \mathcal{W}) = \frac{\partial}{\partial T} (\log c_g), \tag{2.17}$$

where  $d_g/dT \equiv \partial/\partial T + c_g \partial/\partial S$ . For a time-independent basic state, the right-hand side of (2.17) vanishes. Therefore, for a localized wave packet with fixed frequency, (2.17) implies that the value of  $c_g \mathcal{W}$  is conserved following the packet. Therefore, the amplitude of a wave packet can also be obtained from the relation  $c_g \mathcal{W} = \text{constant}$ . The width of the packet must be proportional to  $c_g$  so that the integral of  $\mathcal{W}$  over the packet is conserved.

### 3. One-contour model

#### a. Linear analytic solutions

Consider the simple contour model mentioned in the introduction, consisting of a single PV contour located at  $y = y_1 = 0$ , separating a region of PV with value  $Q_1 = Q$  to the south from a region of PV with value  $Q_2 = Q + \Delta$  to the north. Since  $\Delta = Q_2 - Q_1 = [-U_y]$  (where, as in section 2a, the notation  $[\cdot]$  indicates the jump in a quantity across a contour), the jump in PV is associated with a jump in the wind shear. In the absence of topographic forcing, we then have

$$U(y) = U_0 - (\frac{1}{2})\Delta|y|, \tag{3.1}$$

where  $U_0 = U|_{y=0}$  is a constant. Using (2.5) and (2.6), where here the normal coordinate  $n$  is  $y$  and the tangential coordinate  $s$  is  $x$ , the equation of motion linearized about this basic state is

$$\frac{\partial}{\partial t}([\partial_y \psi]) + \frac{\partial}{\partial x}(U_0[\partial_y \psi]) + \Delta \partial_x \psi = 0 \quad \text{at } y = 0, \tag{3.2}$$

along with

$$\nabla^2 \psi = 0, \quad y \neq 0, \tag{3.3}$$

and the boundary conditions  $|\psi| \rightarrow 0$  as  $|y| \rightarrow \infty$  and  $\psi$  continuous everywhere. Modal solutions have the form  $\psi \propto e^{i(kx - \omega t)} e^{-k|y|}$ , where

$$\omega = U_0 k - \frac{1}{2} \Delta. \tag{3.4}$$

Note that the eddies are isotropic, with  $\langle u^2 \rangle = \langle v^2 \rangle$ , as their zonal and meridional length scales are both equal to  $k^{-1}$ .

In the presence of a zonally varying topographic distribution that is antisymmetric in  $y$ , a flow  $(U_F, V_F)$  is induced upon this single PV contour system with  $V_F = 0$  at  $y = 0$ . The topographically forced steady basic state has a zonal velocity component

$$U(x, y) = U_F(x, y) - \frac{1}{2} \Delta |y|. \tag{3.5}$$

The equations governing the propagation of small-amplitude waves on this flow are (3.2) and (3.3), where  $U_0 = U_F(x, 0)$  is now a function of  $x$ . Note that  $U_0(x)$  occurs inside of the  $x$  derivative in (3.2).

Assuming that  $U_0$  varies on the slow zonal scale  $X = \epsilon x$  where  $\epsilon \ll 1$ , then to order  $\epsilon$ , we seek a modulated wave train solution of the form

$$\psi = \Phi(X) e^{i(kx - \omega t)} e^{-k|y|} + (\text{complex conjugate}). \tag{3.6}$$

Here  $k = k(X)$  is the local wavenumber, and  $\omega$  is constant owing to the time independence of the basic state. The intrinsic frequency,

$$\hat{\omega} \equiv \omega - U_0 k = -\frac{1}{2} \Delta, \tag{3.7}$$

also remains constant as the eddies propagate through the zonally varying flow, and the group velocity

$$c_g \equiv \partial \omega / \partial k = U_0 \tag{3.8}$$

is simply the local basic zonal wind along the contour. The local wavenumber,  $k(X)$ , is proportional to  $U_0^{-1}$ :

$$k(X) = \frac{\omega + \Delta/2}{U_0}. \tag{3.9}$$

The conservation of wave action and (3.6)–(3.8) allow us to predict how the streamfunction amplitude  $|\Phi(X)|$  changes locally. Since, from (2.17) with  $\partial c_g / \partial T = 0$  and  $S \equiv X$ ,

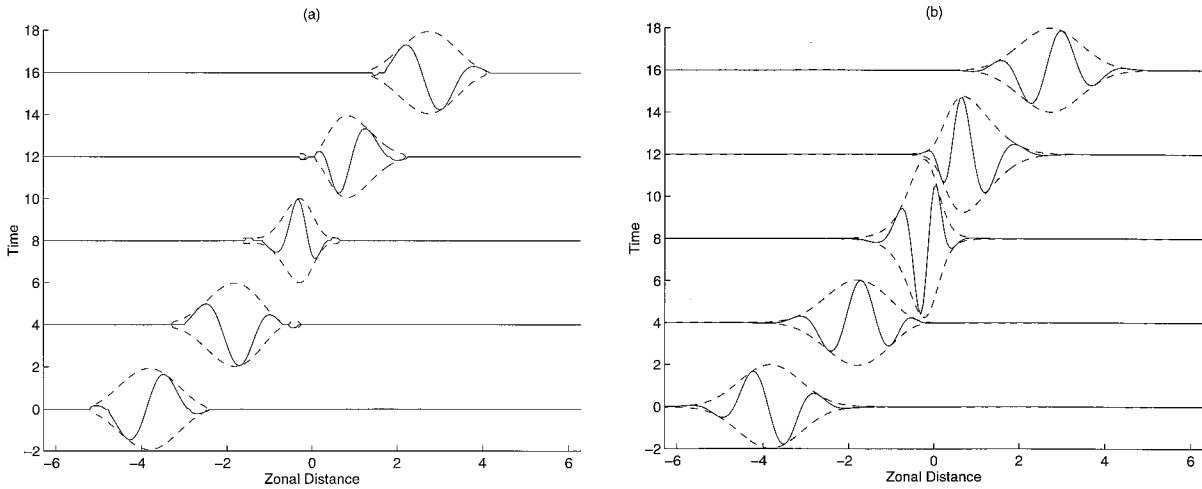


FIG. 2. Evolution of (a) streamfunction  $\psi$  and (b)  $[\partial_y\psi]$  for the linear evolution on the basic flow (3.13). Dashed lines indicate the envelope predicted by the WKB analysis.

$$c_g \mathcal{W} = c_g \frac{\langle E_c \rangle}{\hat{\omega}} = \frac{U_0 \langle E_c \rangle}{-\Delta/2} = \text{const}, \quad (3.10)$$

the phase-averaged energy  $\langle E_c \rangle$  must be proportional to  $U_0^{-1}$ . However, since  $\langle E_c \rangle \propto \langle \psi \eta \rangle \propto k |\Phi|^2$ , it follows from (3.8)–(3.10) that  $|\Phi|^2$  (and hence  $|\Phi|$ ) must be constant on the contour. The same result can be obtained from the order  $\epsilon$  WKB solution presented in appendix C.

The result  $|\Phi| = \text{const}$  on the contour allows for immediate insight into the variation of other dynamical quantities. Specifically, the perturbation particle displacements, which, following (2.7) with  $n = y$ , vary as

$$\langle \eta^2 \rangle^{1/2} = k \langle \psi^2 \rangle_{y=0}^{1/2} / (\Delta/2) \propto U_0^{-1}. \quad (3.11)$$

Particles make larger excursions in regions of weak basic zonal winds. The eddy meridional and zonal wind components  $u$  and  $v$  also scale with  $U_0^{-1}$ , but because their length scale of decay from the contour  $\sim k^{-1} \sim U_0$ , their meridionally integrated variances remain constant.

Because  $\langle E_c \rangle = \hat{\omega} \mathcal{W} = -(\Delta/2) \mathcal{W}$  for the one-contour model, we conclude that the total phase averaged disturbance energy  $\langle \mathcal{E} \rangle$  and, from (2.8), the phase-averaged “generalized enstrophy”  $\mathcal{B}$  are separately conserved. The invariance of  $\langle \mathcal{E} \rangle$  can be seen as a consequence of the fact that eddies are isotropic in the one-contour model. The momentum flux  $\langle uv \rangle$  vanishes owing to the homogeneity of the PV away from the contours, reducing the time tendency for  $\langle \mathcal{E} \rangle$  to

$$\begin{aligned} \frac{d\langle \mathcal{E} \rangle}{dt} &= \int \frac{\partial \left( \frac{1}{2} \langle u^2 + v^2 \rangle \right)}{\partial t} dx \\ &= \iint \frac{1}{2} (\langle v^2 \rangle - \langle u^2 \rangle) \left( \frac{\partial U}{\partial x} - \frac{\partial V}{\partial y} \right) dx dy, \end{aligned} \quad (3.12)$$

where  $v$  is the basic-state meridional velocity compo-

nent. Since the eddies in the one-contour model are isotropic, with  $\langle u^2 \rangle = \langle v^2 \rangle$  everywhere,  $\langle \mathcal{E} \rangle$  is conserved.

### b. Numerical simulations

#### 1) LINEAR CALCULATIONS

To explore the results of the previous section while retaining the assumption of linearity, we numerically solve (3.2). The solution method consists of using the Fourier transform to relate  $\psi$  to  $[\partial_y\psi]$  as well as to calculate the  $x$  derivatives, and numerically integrating (3.2) with leapfrog time stepping, along with periodic application of an Euler backward time step to damp the computational mode. This method allows examination of linear wave-packet propagation through arbitrary zonally varying basic flows.

We consider a wave propagation problem in which there is relatively little scale separation between the wave and the basic-state flow in order to strain the validity of the WKB theory. The zonally varying basic flow we examine is

$$U_0(x) = 1 - \frac{1}{2} \exp\left(\frac{-x^2}{4}\right), \quad (-5\pi \leq x \leq 5\pi), \quad (3.13)$$

where we take the PV jump  $\Delta$  to be unity. Upon this basic flow we superpose an initial disturbance of the form

$$[\partial_y\psi] = \exp\left[\frac{-(x-x_0)^2}{4}\right] \exp(ikx) \quad (3.14)$$

far from the weak flow region, where we take  $k = 2$ , which, applying (3.4), yields  $\omega = 1.5$ . The evolution of the disturbance fields  $\psi$  and  $[\partial_y\psi] \propto \eta$  with time is shown in Fig. 2. The disturbance wavenumber and amplitude variations resulting from interaction with the zonally

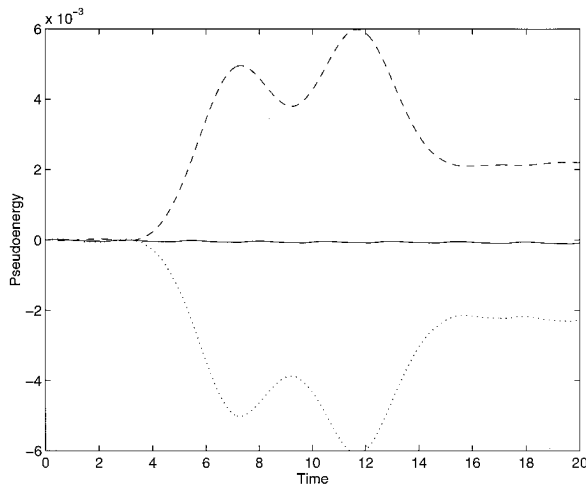


FIG. 3. Deviation of pseudoenergy components  $\mathcal{E}$  (dashed) and  $\mathcal{B}$  (dotted), as well as the pseudoenergy  $\mathcal{A} = \mathcal{E} + \mathcal{B}$  (solid), from their individual base values.

varying basic state agree remarkably well with the WKB solutions, despite the fact that the basic flow varies on a similar scale to the packet eddies. The maximum streamfunction amplitude remains constant to within 2% as the packet propagates through the zonally varying flow, and the particle displacements scale like  $U_0^{-1}$  as predicted, increasing by a factor of 2 at the flow minimum.

Deviations in the domain-integrated wave action,  $\int \langle \langle E_c \rangle / \hat{\omega} \rangle dx$ , are of the order of 0.5% of its initial value as the packet propagates through the weak flow region. These deviations are the result of local violations of the WKB assumptions. On the other hand, deviations in the pseudoenergy  $\langle \mathcal{A} \rangle$ , which is conserved independently of the WKB approximation, are shown in Fig. 3 to be negligible to within the accuracy of the numerical discretization. This is because of cancellation between the two pseudoenergy components  $\langle \mathcal{E} \rangle$  and  $\langle \mathcal{B} \rangle$ , which individually have deviations from their initial values of the same order of magnitude as the deviations in the domain-integrated wave action. Clearly, the leading-order WKB theory and wave action conservation provide an almost complete characterization of linear disturbances in the one-contour model.

## 2) NONLINEAR CALCULATIONS

As the amplitude of the disturbance to the one-contour model increases, at some point nonlinear effects such as wave breaking will become important. To study nonlinear effects on the propagation of waves for the one-contour model, the numerical method of contour dynamics and surgery (CS) has been used to obtain high-resolution solutions of (2.3) (Dritschel 1988, 1989a). This method has been used in a similar context recently by Polvani and Plumb (1992), Waugh et al. (1994), Nakamura and Plumb (1994), and Pieters and

Waugh (1996) to study wave propagation and breaking on similar low-order contour models, and it has been shown that such calculations reproduce some aspects of wave breaking in the atmosphere.

In CS, the velocity at a point  $\mathbf{x}$  is given by

$$\mathbf{u}(\mathbf{x}) = -\pi \sum_{j=1}^N \Delta_j \oint_{C_j} G(\mathbf{x} - \mathbf{x}_j) d\mathbf{x}_j + \mathbf{u}_F(\mathbf{x}), \quad (3.15)$$

where  $G$  is the Green's function for Poisson's equation in the domain of interest,  $\mathbf{u}_F$  is the velocity due to the topographic forcing, and  $C_j$  is the  $j$ th PV contour. The material conservation of PV ensures that it will remain piecewise constant, and its subsequent evolution is then completely determined by the advection of the contours. The computational details of this procedure follow Dritschel (1988, 1989a); briefly, each contour is numerically represented by a series of computational nodes that are advected by the velocity field (3.15). To preserve the resolution of the calculation, the positions of these nodes are continually adjusted, with nodes added in regions of high curvature. To enable efficient longtime integrations, filamentary structures smaller than some cutoff scale are removed using Dritschel's surgery procedure. The equations of motion are solved in a domain that is  $10\pi$  periodic in  $x$  and unbounded in  $y$ ; the details of the solutions herein are not sensitive to the choice of the domain width, provided it is large enough.

To create the zonally varying flow, we introduce topography in the form of two point vortices,

$$H(x, y)/H_{\text{ref}} = \sum_{j=1}^2 H_j \delta(\mathbf{x} - \mathbf{x}_j)/H_{\text{ref}}, \quad (3.16)$$

where  $\mathbf{x}_j$  is the vortex location and  $\delta$  is the Dirac delta function. If these vortices are of equal but opposite strength and are positioned symmetrically about  $y = 0$ , the basic-state meridional velocity will vanish along the PV contour.

We choose the topographic vortex strength to be  $|H_{1,2}|/H_{\text{ref}} = 4.08$  and locate the vortices at  $(x, y) = (0, \pm 5/2)$ . With a PV jump  $\Delta = 1$  and adding an overall uniform zonal velocity component of 1.031 (which differs from unity due to the periodic domain), we obtain a velocity field with unit maximum zonal wind that weakens by a factor of 2 at the center of the domain. The basic flow along-contour velocity and streamfunction are shown in Fig. 4. The initial contour displacement for all one-contour integrations herein is

$$\eta(x) = \eta_0 \exp\left[\frac{-(x - x_0)^2}{4}\right] \cos(k_0 x + \chi), \quad (3.17)$$

where  $\eta_0$  is the initial amplitude,  $\chi$  is a phase factor,  $x_0 = -5\pi$  is the packet's initial position, and  $k_0 = 2$  is the packet's initial wavenumber. In the nonlinear calculations,  $\eta_0$  is varied to explore the effects of nonlinearity on the packet evolution, and the phase factor  $\chi$

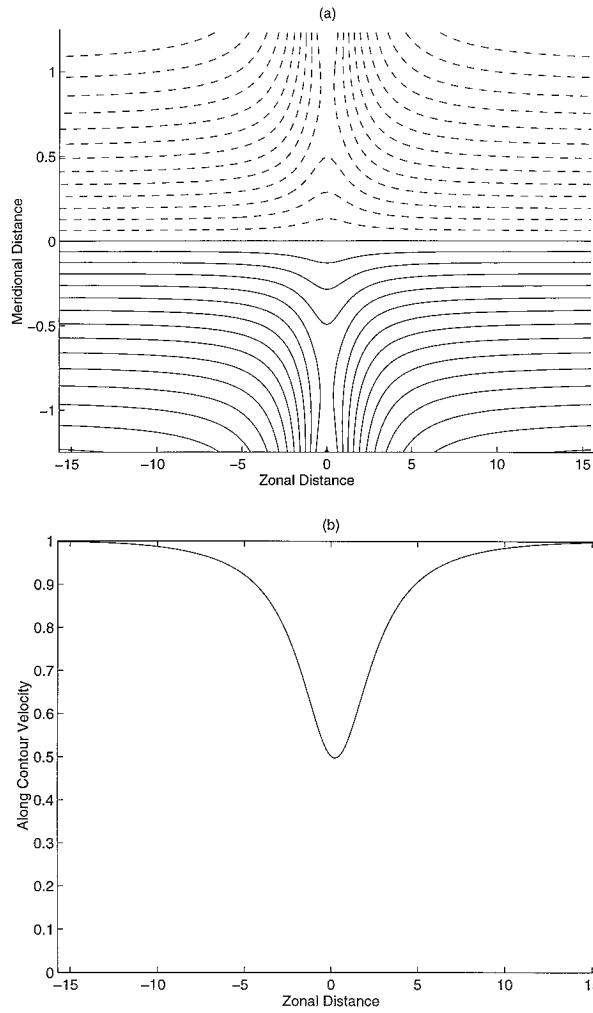


FIG. 4. (a) Streamfunction and (b) along-contour velocity for the one-contour case considered in this subsection. The contour interval in (a) is  $2.5 \times 10^{-2}$ .

is varied to explore the effect of the initial phase of the wave. Some phase dependence is to be expected when the scale separation between the wave and the basic-state flow is modest, as is the case in our example.

In order to properly interpret the nonlinear calculations, it is desirable to understand how large  $\eta_0$  must be for wave breaking to occur. As Polvani et al. (1989) and Polvani and Plumb (1992) found in their studies of wave breaking in contour distributions, breaking occurs when, in the reference frame associated with the phase velocity of the wave, a stagnation point approaches the perturbed contour. Neglecting transients, simple kinematics indicate that flow about the stagnation point will pinch off wave material, causing the wave to break.

For the present case, such a stagnation point first occurs when the perturbed contour is farthest from the rest contour, that is, at a wave crest or trough. As the perturbation meridional velocity vanishes at wave crests and troughs, the criterion for a stagnation point at such points is

$$U(x, y) + u = c_{ph}, \tag{3.18}$$

where

$$U(x, y) \approx U_0(X) - (\frac{1}{2})\Delta|y| \tag{3.19}$$

is the basic-state zonal wind near the contour,  $u$  is the perturbation zonal wind, and the  $c_{ph}$  is the phase speed for the one-contour model, which can be obtained approximately from the linear dispersion relation (3.4):

$$c_{ph} = U_0(X) - (\frac{1}{2})\Delta/k. \tag{3.20}$$

The approximation used in (3.19) holds for points close to the contour and makes a negligible difference in the calculation to follow.

Consider perturbation particle displacements with the local form

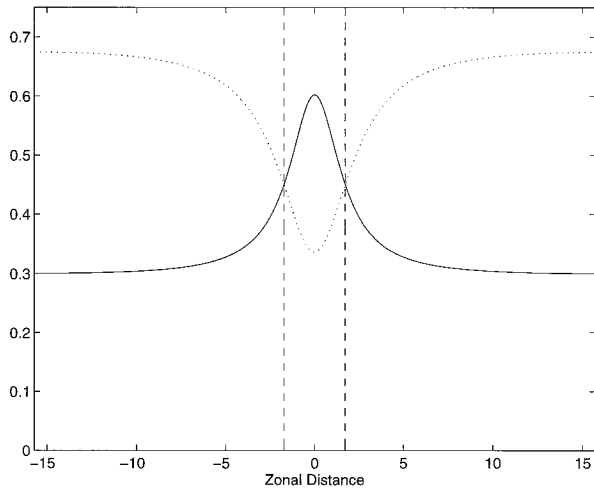


FIG. 5. Plot of  $|\eta_{cr}|$  (dotted) and  $|\eta_{max}|$  (solid) for initial amplitude  $\eta_0 = 0.3$ , as described in text. Breaking expected in region  $|x| \leq x_b \approx 1.73$ , where the location of  $\pm x_b$  is denoted by the dashed lines.

$$\eta = |\eta_{cr}| \cos(kx - \omega t), \quad (3.21)$$

where  $|\eta_{cr}|$  is the minimum magnitude at which breaking will occur for a given  $U_0$ ,  $\Delta$ , and  $k$ . Using (2.7) and (3.6), the perturbation zonal velocity has the form

$$u = -\partial_y \psi = (\frac{1}{2})\Delta |\eta_{cr}| \cos(kx - \omega t) e^{-k|y|}. \quad (3.22)$$

Substituting (3.19), (3.20), and (3.22) evaluated at a wave crest into (3.18) and simplifying, we arrive at the following expression:

$$k|\eta_{cr}| (1 - e^{-k|\eta_{cr}|}) = 1, \quad (3.23)$$

which has the immediate solution

$$k|\eta_{cr}| \approx 1.35. \quad (3.24)$$

As indicated in (3.9) and (3.11), linear theory predicts that both the maximum particle positions  $|\eta_{max}| = \sqrt{2}\langle \eta^2 \rangle^{1/2}$  and the local wavenumber  $k$  vary as  $U_0^{-1}$ . Hence, as  $U_0$  becomes smaller, breaking occurs closer to the basic-state contour at  $y = 0$ . Figure 5 shows the variation of  $|\eta_{cr}|$  from (3.24) for the basic-state flow  $U(x, y)$  of Fig. 4, where we take the local wavenumber to be  $k = 2$  at the basic-state flow maximum. Using (3.24) and (3.9), the minimum value of  $|\eta_{cr}|$  is found to be  $|\eta_{cr}|_{min} \approx 0.338$  for the present choice of basic-state and wave parameters. For reference, the linear theory maximum particle displacements  $|\eta_{max}|$  from (3.11) for initial particle displacement amplitude  $\eta_0 = 0.3$  are also shown in the figure. Breaking is expected in the region where  $|\eta_{max}| > |\eta_{cr}|$ , which in this example occurs for  $|x| \leq x_b \approx 1.73$ .

For this basic-state flow and wavenumber, Eq. (3.24) predicts that breaking will occur when  $\eta_0 \geq 0.169$ . The nonlinear simulations confirm this expectation, as we find that for  $\eta_0 \leq 0.165$ , the waves behave quasi-linearly and do not break. The breaking observed for  $\eta_0 \geq 0.17$  is not the familiar roll-up of PV contours associated

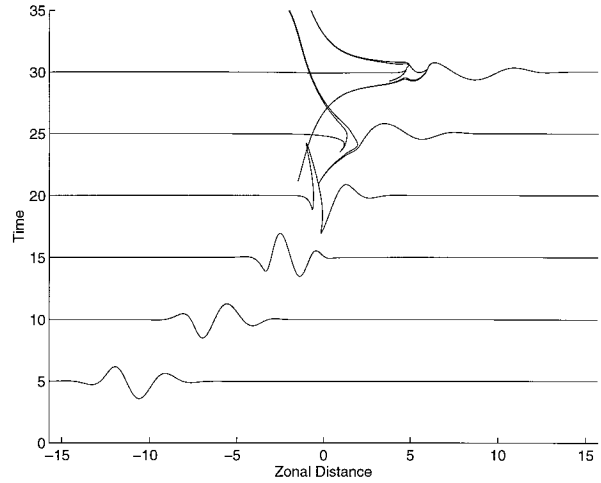


FIG. 6. Time evolution of the  $\eta_0 = 0.4$  case for the one-contour storm track.

with Rossby wave critical layers in a continuous PV distribution (Warn and Warn 1978), but instead is characterized by the development of filaments of PV. This is apparent in the time evolution of an  $\eta_0 = 0.4$  simulation shown in Fig. 6. This shedding of PV filaments is a common signature of wave breaking in nondivergent barotropic contour dynamics simulations (Dritschel 1988; Polvani and Plumb 1992) and arises because the strain of the large-scale flow overcomes the local tendency of the vorticity to roll up (Dritschel 1989b).

The nonlinearity associated with the wave breaking and the shedding of PV filaments changes the structure of the wave-packet eddies. Consider the final maximum meridional particle displacement amplitude  $\eta_f$  of the wave portion of the packet (as opposed to the filament portion, as outlined in Fig. 7) after exiting the weak flow region. Figure 8a shows  $\eta_f$  for  $\eta_0$  in the range  $[0.025, 0.5]$ . For each  $\eta_0$ , simulations for four values of the initial phase  $\chi = (0, \pi/4, \pi/2, 3\pi/4)$  have been performed to illustrate the phase dependence of the wave breaking. The figure shows that  $\eta_f$  is never larger than a maximum value of approximately 0.25, whatever the value of  $\eta_0$ . In effect, the wave packets have had their amplitudes attenuated, or “clipped,” to a maximum value by the wave breaking.

We propose a simple hypothesis to explain the maximum value of  $\eta_f$  observed in the simulations. This hypothesis is that the maximum particle displacements are clipped nonconservatively to the minimum stagnation point distance  $|\eta_{cr}|_{min}$ , but otherwise undergo conservative linear modulation as usual. Explicitly, we integrate the equation.

$$\frac{\partial}{\partial x}(c_g W) \propto \frac{\partial}{\partial x}(U_0^2 \langle \eta^2 \rangle) = 0 \quad (3.25)$$

for increasing  $x$ , with the proviso that the particle dis-

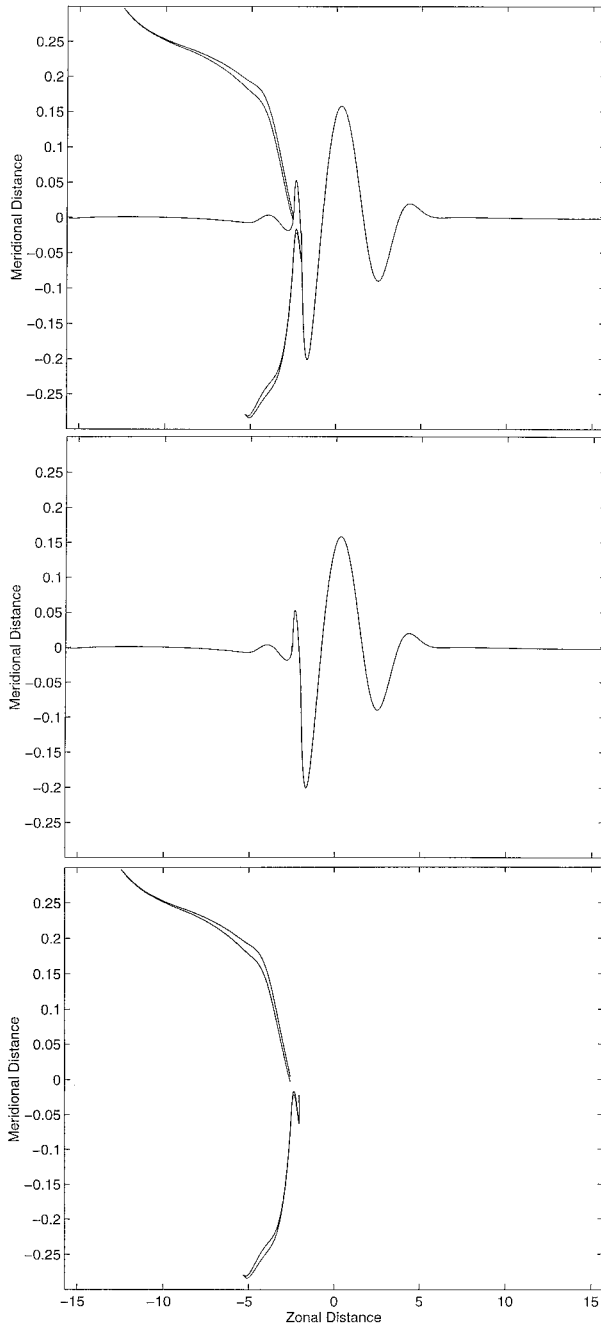


FIG. 7. Decomposition of a typical solution (top) into wave (middle) and filament (bottom) components.

placements are clipped to  $|\eta_{cr}|$  whenever  $|\eta| > |\eta_{cr}|$  locally. For the initial disturbance (3.17), and this basic state, for which  $U_0$  has a minimum at  $x = 0$ , this implies that

$$\eta_f = \min\left(\frac{\eta_0 U_0(-\infty)}{U_0(+\infty)}, \frac{|\eta_{cr}|_{\min} U_0(0)}{U_0(+\infty)}\right), \quad (3.26)$$

where the notation  $\mp\infty$  denotes values of quantities in the regions well upstream and well downstream of the region of breaking, respectively. An illustration of this clipping with linear modulation is shown in Fig. 9. Figure 8b shows the numerical experiments along with the prediction from (3.26), which, with  $|\eta_{cr}|_{\min} \approx 0.338$ , yields a maximum value for  $\eta_f$  of approximately 0.169. (Note that this is the same estimated value as the estimated minimum initial amplitude,  $\eta_0$ , for the onset of breaking.) The clipping hypothesis provides a reasonable estimate of the amount of attenuation associated with wave breaking in all cases. The estimated  $\eta_f$  tends to be too large for the small  $\eta_0$  cases and too large for the large  $\eta_0$  cases. This mechanism and the estimate of the final amplitude may be a useful way to characterize and parameterize upper-tropospheric wave breaking.

Clipping also results in a significant irreversible loss of wave action. For example, for  $\eta_0 = 0.3$  and  $|\eta_{cr}|_{\min} \approx 0.338$ , (3.26) predicts that the domain-integrated wave action associated with the wavy part of the flow will decrease by

$$\frac{\int_{\text{final}} w dx}{\int_{\text{initial}} w dx} = \frac{|\eta_{cr}|_{\min}^2}{\{U(-\infty)\eta_0/U(0)\}^2} \approx 0.321. \quad (3.27)$$

This prediction can be compared to the actual loss of wave action directly calculated from the four  $\eta_0 = 0.3$  numerical integrations using the wave/filament decomposition illustrated in Fig. 7. From these integrations, we find  $0.26 \leq \int_{\text{final}} w dx / \int_{\text{initial}} w dx \leq 0.54$ . This loss of wave action from the wavy part of the flow may be attributed to the generation of filaments.

Another interesting aspect of the simulations in which wave breaking occurs is that the disturbance wavelength has increased markedly after exiting the weak flow region. Figure 10 shows that the final disturbance wavelength increases as the initial amplitude of the packets is increased above the critical breaking amplitude. For the  $\eta_0 = 0.4$  integration with  $\chi = 0$ , the final disturbance wavelength is double that of the  $\eta_0 = 0.1$  integration with  $\chi = 0$ , which behaves more or less linearly. Since the disturbances are still wave-like away from the breaking region, the dispersion relation still holds, yielding  $k = (\omega + \Delta/2)/U_0(x)$ , where  $U_0(x)$  is approximately constant and equal to its value at  $x = -5\pi$ . Hence, we conclude that the irreversible decrease in  $k$  due to the breaking is associated with a corresponding irreversible decrease in the frequency  $\omega$ . This reduction in frequency is intriguing and suggests a mechanism relating low-frequency variability and regions where the jet strength is weak, a relation that is well established observationally (Wallace and Blackmon 1983).

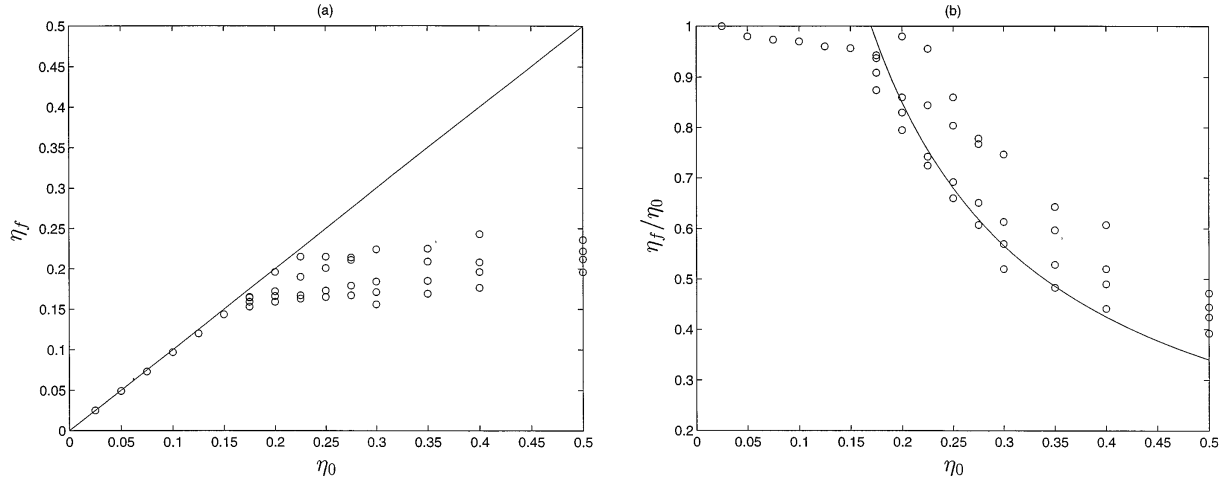


FIG. 8. (a) Final wave amplitude  $\eta_f$  versus initial wave amplitude  $\eta_0$  for one-contour model simulations. The scatter for each value of  $\eta_0$  is the result of simulations with different initial wave phases. Also shown is the line  $\eta_0 = \eta_f$ . (b) Ratio  $\eta_f/\eta_0$  (circles) as a function of  $\eta_0$  along with the prediction (solid) given by the clipping hypothesis described in the text.

#### 4. Two-contour model

The next member of the contour model hierarchy is the two-contour model, consisting of three regions of homogeneous barotropic PV, separated by two zonally varying PV contours. The presence of a second contour adds two features absent in the one-contour model. First, since the basic-state contours are streamlines, the contour separation is proportional to the strength of the zonal flow, and hence the effective PV gradient given by the contour separation is also proportional to the strength of the zonal flow. Second, eddies are anisotropic in the two-contour model. These features make the two-contour model a more realistic representation of wave propagation in the upper troposphere than the one-contour model.

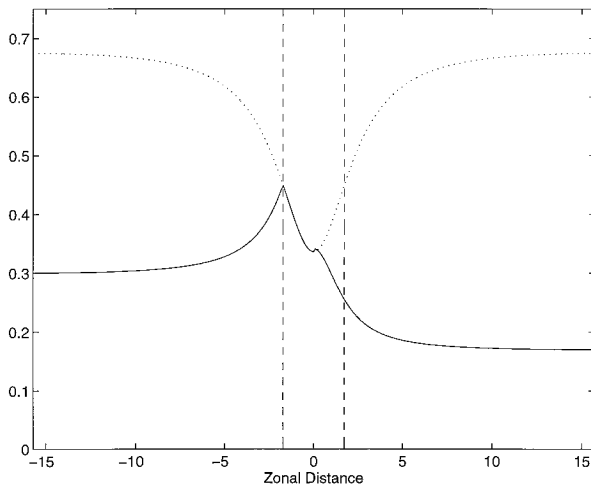


FIG. 9. Plot of  $|\eta_{cr}|$  (dotted) and  $|\eta_{max}(x)|$  (solid) for initial amplitude  $\eta_0 = 0.3$  assuming clipping to linear theory critical lines, as described in text. Clipping occurs in the region  $-x_b \leq x \leq 0$ , where  $x_b \approx 1.73$ . The location of  $\pm x_b$  is denoted by the dashed lines.

#### a. Linear analytic solutions

The simplest two-contour model consists of two contours located symmetrically about the meridional origin at  $y = y_1 = -y_0(x)$  and  $y = y_2 = +y_0(x)$ , each marking a PV jump  $\Delta_1 = \Delta_2 = \Delta > 0$ . In the absence of topographic forcing,  $y_0(x)$  is constant, and the basic-state wind is zonal and given by

$$U(y) = \begin{cases} U_0 - \Delta|y - y_0|, & y > y_0 \\ U_0, & -y_0 \leq y \leq y_0 \\ U_0 - \Delta|y + y_0|, & y < -y_0, \end{cases} \quad (4.1)$$

where  $U_0$  is a constant.

To facilitate comparison with the one-contour model results, we seek solutions to the linearized equations of motion (2.6) that have streamfunction symmetric about  $y = 0$ . Vanishing of the perturbation PV away from the contours (2.5), along with the boundary conditions  $|\psi| \rightarrow 0$  as  $|y| \rightarrow \infty$  and  $\psi$  continuous everywhere, yields

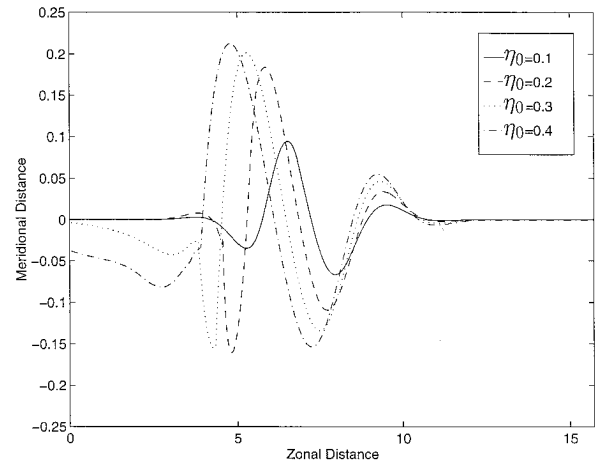


FIG. 10. "Wave" portion of the contour displacements at  $t = 27.5$  for the one-contour case as a function of initial amplitude  $\eta_0$ .

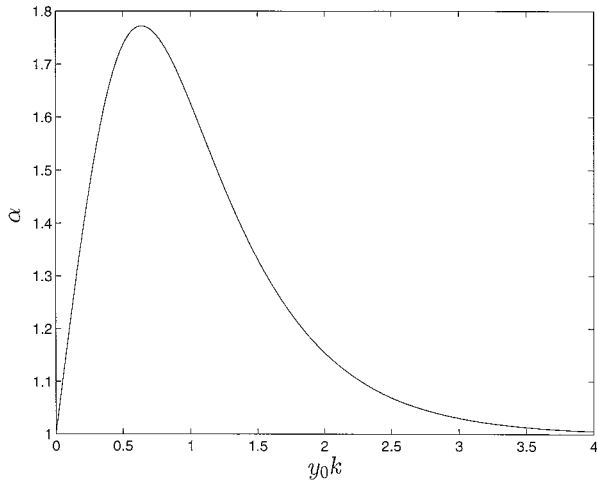


FIG. 11. Anisotropy index  $\alpha$  for the two-contour system.

a symmetric modal solution of the form  $\psi = \hat{\psi}(y)e^{i(kx - \omega t)}$  + complex conjugate, where

$$\hat{\psi}(y) = \begin{cases} e^{-ky - y_0} & y < -y_0 \\ \cosh(ky)/\cosh(ky_0) & -y_0 \leq y \leq y_0 \\ e^{-ky + y_0} & y > y_0 \end{cases} \quad (4.2)$$

Substituting this solution form into the linear equations of motion (2.6) then gives the dispersion relation

$$\omega = U_0 k - (\frac{1}{2})\Delta(1 + e^{-2y_0 k}). \quad (4.3)$$

The quantity  $y_0 k$  in (4.3) measures the weakness of the coupling between the contours. For  $y_0 k \gg 1$ , (4.3) reduces to the one-contour dispersion relation (3.4) with a PV jump of  $\Delta$ , and the eigenfunction  $\hat{\psi}(y)$  in (4.2) decays exponentially on both sides of each contour; the contours are uncoupled, apart from sharing a common disturbance frequency and wavelength. For  $y_0 k \ll 1$ , (4.3) reduces to the one-contour dispersion relation with a PV jump of  $2\Delta$ , and the eigenfunction  $\hat{\psi}(y)$  is approximately constant between the contours and decays exponentially away from them; the two contours are strongly coupled and act effectively as a single contour.

Unlike one-contour model eddies, eddies in the two-contour model are not isotropic. One measure of eddy anisotropy is the quantity

$$\alpha = \frac{\int_{-\infty}^{\infty} \langle v^2 \rangle dy}{\int_{-\infty}^{\infty} \langle u^2 \rangle dy}, \quad (4.4)$$

where eddies with  $\alpha > 1$  are meridionally extended and zonally compressed. For symmetric modes in the two-contour model, we have

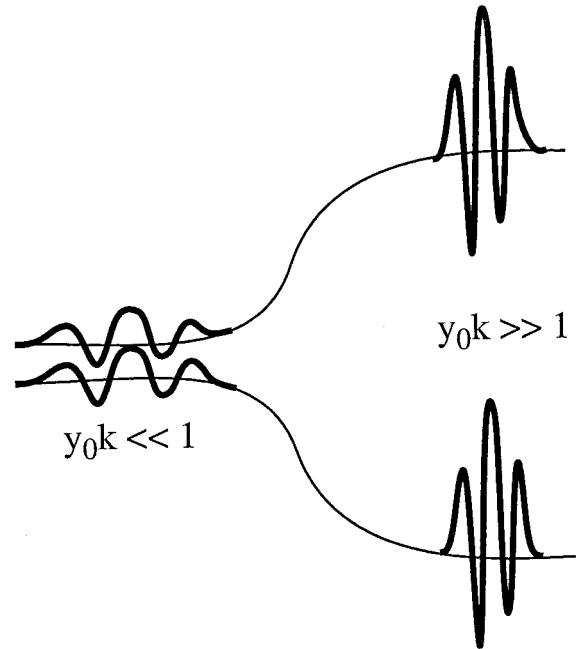


FIG. 12. Transition from an equivalent one-contour to a two-contour system. The dark lines indicate particle positions in the coupled region where  $y_0 k \ll 1$  and in the uncoupled region where  $y_0 k \gg 1$ .

$$\alpha = \frac{\sinh(2y_0 k)/2 + y_0 k + \cosh^2(y_0 k)}{\sinh(2y_0 k)/2 - y_0 k + \cosh^2(y_0 k)} \geq 1. \quad (4.5)$$

As shown in Fig. 11, in the tightly coupled limit  $y_0 k \rightarrow 0$ , as well as in the limit in which the contours are independent  $y_0 k \rightarrow \infty$ , the eddies are nearly isotropic. Once again, the two-contour model reduces to the one-contour model in both the weakly and strongly coupled limits. Eddy anisotropy peaks at  $\alpha \approx 1.75$  for a moderate value of the coupling  $y_0 k \approx 0.63$ .

Because the two-contour model behaves like the one-contour model for both weak and strong coupling, the one-contour model wave action analysis of section 3 can be used to analyze wave propagation through a zonally varying two-contour flow in the following thought experiment. Consider a linear wave packet that propagates from a region where the two contours are tightly coupled ( $y_0 k \ll 1$ ) into a region where they are completely uncoupled ( $y_0 k \gg 1$ ), as illustrated schematically in Fig. 12. Assuming each contour marks a PV jump of  $\Delta$ , where the contours are tightly coupled, they will act as if they were a single contour with PV jump  $2\Delta$ . This effective one-contour system will have wave action  $\mathcal{W}_{\text{coupled}} = \int \langle E_{c,\text{coupled}} \rangle / \Delta dx$ , where the eddy energy  $\langle E_{c,\text{coupled}} \rangle \approx k_{\text{coupled}} \langle \psi_{\text{coupled}}^2 |_{y=y_0} \rangle$  follows from the one-contour results of section 3a. Where the contours are widely separated, they will act as two independent one-contour systems, each with PV jump  $\Delta$ .

In this region, each contour will have wave action  $W_{\text{uncoupled}} = \int \langle E_{c,\text{uncoupled}} \rangle / (\Delta/2) dx$ , where  $\langle E_{c,\text{uncoupled}} \rangle \approx k_{\text{uncoupled}} \langle \psi_{\text{uncoupled}}^2 |_{|y|=y_0} \rangle$  is the eddy energy on each of the two independent contours.

Conservation of wave action requires

$$2 \int \langle E_{\text{uncoupled}} \rangle / (\Delta/2) dx = \int \langle E_{\text{coupled}} \rangle / \Delta dx \quad (4.6)$$

or  $\int \langle E_{\text{uncoupled}} \rangle dx = 1/4 \int \langle E_{\text{coupled}} \rangle dx$ . The eddy energy on each of the uncoupled contours is one-fourth the eddy energy in the tightly coupled region, implying a halving of the total eddy energy from its initial value. The other half of the energy has been transferred to the mean flow. This result shows that unlike the one-contour model, the two-contour model's wave action and eddy energy are not equivalent; the former is conserved during propagation through the zonally varying basic state, while the latter is not. The loss in eddy energy is associated with the anisotropy of the two-contour eddies [cf. (3.12)] as they pass through the intermediate region where  $y_0 k \sim 1$  and  $\partial_x U_0 < 0$ , since  $\langle v^2 \rangle > \langle u^2 \rangle$  between the contours in this region.

For this thought experiment, conservation of wave action implies modulations in the eddy streamfunction of the form

$$\frac{|\Phi_{\text{uncoupled}}|}{|\Phi_{\text{coupled}}|} \approx \frac{1}{2} \left( \frac{\omega + \Delta}{\omega + \Delta/2} \right)^{1/2} \quad (4.7)$$

and particle displacement modulations

$$\frac{|\eta_{\text{uncoupled}}|_{\text{max}}}{|\eta_{\text{coupled}}|_{\text{max}}} \approx \frac{U_{\text{coupled}}}{U_{\text{uncoupled}}} \left( \frac{\omega + \Delta}{\omega + \Delta/2} \right)^{-1/2}. \quad (4.8)$$

Although the eddy energy and the streamfunction decrease somewhat on each contour, the particle displacements are greatly amplified in the region of weak flow, just as in the one-contour case. Hence, it is expected that initially small amplitude waves will break most easily in the weak flow region.

To understand wave propagation in the two-contour model more generally for all values of  $y_0 k$ , we follow the procedure of section 3a and assume a slowly zonally varying basic-state wind  $U(X)$  with modulated wave train perturbations of the form

$$\psi = \Phi(X) \hat{\psi} e^{i(kx - \omega t)} + \text{complex conjugate}. \quad (4.9)$$

Here,  $\hat{\psi}$  and  $\omega$  are respectively given by (4.2) and (4.3), and  $k$ ,  $y_0$ , and  $U_0$  are all functions of the slow spatial scale  $X$ . In contrast to the one-contour case, the two-contour symmetric mode intrinsic frequency

$$\hat{\omega} = -(1/2)\Delta(1 + e^{-2y_0 k}) \quad (4.10)$$

is not independent of the basic flow, and the two-contour symmetric mode group velocity

$$c_g \equiv \partial \omega / \partial k = U_0 + \Delta y_0 e^{-2y_0 k} \quad (4.11)$$

is not simply the local basic-state zonal wind, but exceeds it by an amount dependent on  $y_0$ ,  $\Delta$ , and  $k$ . The

functional dependence of  $c_g$  upon  $k$  indicates that initially localized wave packets will spread with time.

For two-contour symmetric modes (4.2), the phase-averaged energy associated with each contour is

$$\langle E_c \rangle = (1/2)k(1 + \tanh(y_0 k)) \langle \psi^2 |_{|y|=y_0} \rangle. \quad (4.12)$$

Wave action conservation then implies

$$c_g \mathcal{W} = c_g \frac{2 \langle E_c \rangle}{\hat{\omega}} = -\frac{4(U_0 k + \Delta y_0 k e^{-2y_0 k}) \langle \psi^2 |_{|y|=y_0} \rangle}{\Delta(1 + e^{-2y_0 k})^2} = \text{const}, \quad (4.13)$$

which, after some algebra, gives

$$|\Phi(X)| \propto \langle \psi^2 |_{|y|=y_0} \rangle^{1/2} \propto \frac{1 + e^{-2y_0 k}}{\left( \omega + \frac{1}{2}\Delta[1 + (1 + 2y_0 k)e^{-y_0 k}] \right)^{1/2}}. \quad (4.14)$$

It may be shown that this result also follows directly from an order  $\epsilon$  WKB solution after a calculation along the lines of that in appendix C (but much more laborious). Taking the limits of weak and strong coupling, the thought experiment results (4.7) and (4.8) may be easily recovered from this solution.

## b. Numerical simulations

### 1) LINEAR CALCULATIONS

In section 4a we emphasized the strongly coupled ( $y_0 k \gg 1$ ) and weakly coupled ( $y_0 k \ll 1$ ) regimes of the two-contour model, in which the two-contour model behaved essentially like the one-contour model. We begin this section by considering the behavior of a wave packet propagating from a strongly coupled region into an intermediate region ( $y_0 k \sim 1$ ). In the intermediate regime, which cannot be represented by the one-contour model, eddy anisotropy becomes important and eddy energy is no longer conserved.

The particular basic-state along-contour velocity  $U_0$  and contour positions  $\pm y_0(x)$  we use for the numerical integrations are shown in Fig. 13. The mean flow is reduced by a factor of 4 at the jet minimum (see caption for details). The steady basic states for the zonally varying two-contour distributions are found using iterative relaxation of the PV contours (Pierrehumbert 1980). Given  $U_0(x)$  and  $y_0(x)$ , and a value of  $k$  at a particular point, (4.3) can be used to calculate numerically the  $x$  dependence of  $k$ , and hence the streamfunction and particle position amplitudes from the wave action solution (4.14). In this case,  $y_0|_{x=\pm 5\pi}$  and  $k|_{x=\pm 5\pi}$  were chosen to represent highly coupled contour waves at the zonal flow maximum. Figure 14a shows the variation in the scaled wavenumber  $k/k|_{x=\pm 5\pi}$ , the scaled streamfunction amplitude  $|\Phi|/|\Phi|_{x=\pm 5\pi}$ , and the scaled particle position amplitude  $|\eta|_{\text{max}}/|\eta|_{\text{max},x=\pm 5\pi}$  where  $y_0|_{x=\pm 5\pi} = 0.025$  and  $k|_{x=\pm 5\pi} = 2$ . Figure 14b

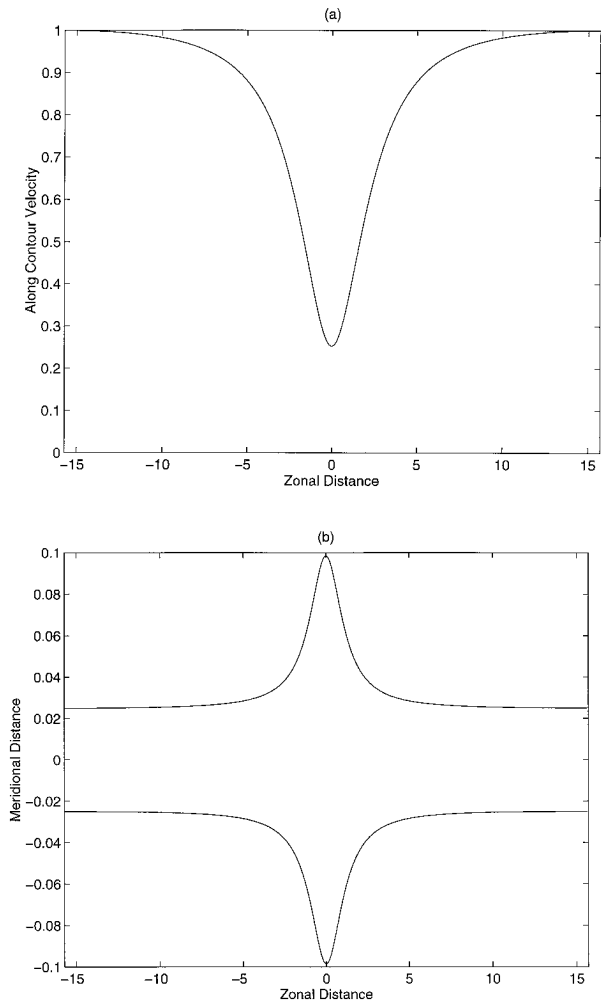


FIG. 13. (a) Basic-state along-contour velocity and (b) contour positions for the linear two-contour case example. Each PV contour marks a PV jump of  $\Delta = 1/2$ , and the strength of the topographic forcing at  $(x, y) = (0, \pm 5/2)$  has been increased over that of section 3b to  $|H_0|/H_{\text{ref}} \approx 5.825$ , so that the minimum along-contour velocity (which occurs at  $x = 0$ ) is one-quarter of its maximum value.

shows the variation in the anisotropy  $\alpha$  and the contour coupling  $y_0 k$ .

As in the one-contour case, the wavenumber  $k$  increases strongly in the weak flow region, although not by a full factor of 4 as it would were this a one-contour system. As shown in Fig. 14b, the contour coupling  $y_0 k$  increases by a factor of  $\approx 16$  at the weak flow region from  $(y_0 k)|_{x=-5\pi} \approx 0.05$  to  $(y_0 k)|_{x=0} \approx 0.8$ , leading to an increase in the eddy anisotropy  $\alpha$  from a reasonably isotropic value of  $\alpha \approx 1.1$  at  $x = \pm 5\pi$  to a strongly anisotropic value of  $\alpha \approx 1.75$  at  $x = 0$  where the basic-state zonal flow is weakest. The WKB solution indicates that this increase in anisotropy leads to a decrease in the along-contour streamfunction amplitude by 35% in the weak flow region. However, the approximate increase in  $k$  with  $U_0^{-1}$  still dominates the

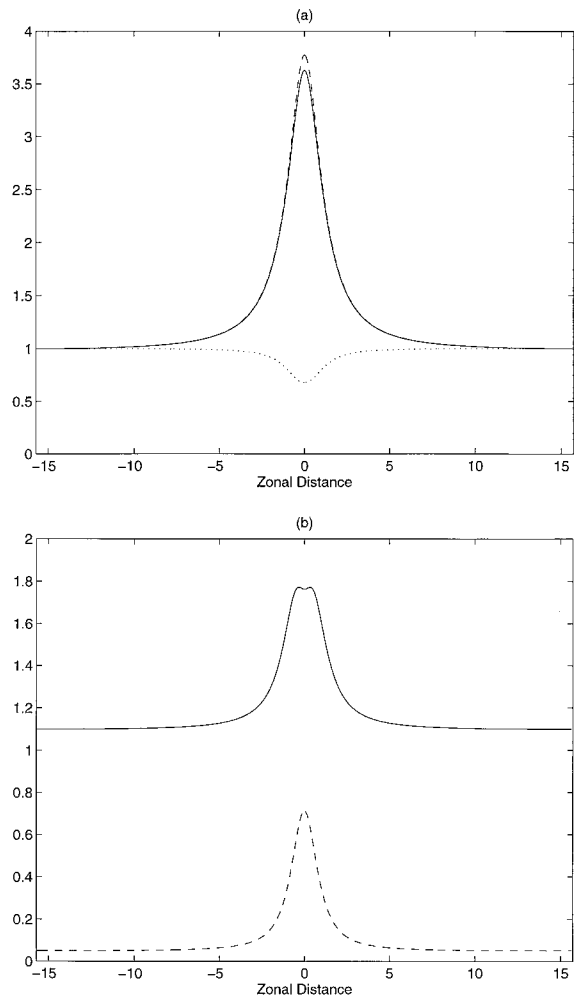


FIG. 14. (a) Scaled variations in wavenumber  $k$  (solid),  $\eta$  (dashed), and  $\psi$  (dotted) for the linear two-contour case example. (b) Variations in anisotropy  $\alpha$  (solid) and contour coupling  $y_0 k$  (dashed) for the linear two-contour case example.

variation in the particle displacements where the flow is weak, leading to an increase in the particle displacements by a factor of approximately 3.5 at the flow minimum. This is consistent with the general principle that particle displacements are largest in regions of weak PV gradients.

The zonally varying contours do not allow direct solution of the linear equations of motion (2.6) using one-dimensional spectral methods. In order to test the validity of the WKB theory, we therefore compare the WKB solutions to contour dynamics integrations using small amplitude waves with initial amplitude  $\eta_0 = 0.025$ . Figure 15 shows that the WKB solution accurately represents the modulation of the particle positions and streamfunction, although variations in the actual particle positions and streamfunction are approximately 10% stronger than the WKB theory would suggest. The WKB solution appears to break down sooner in this

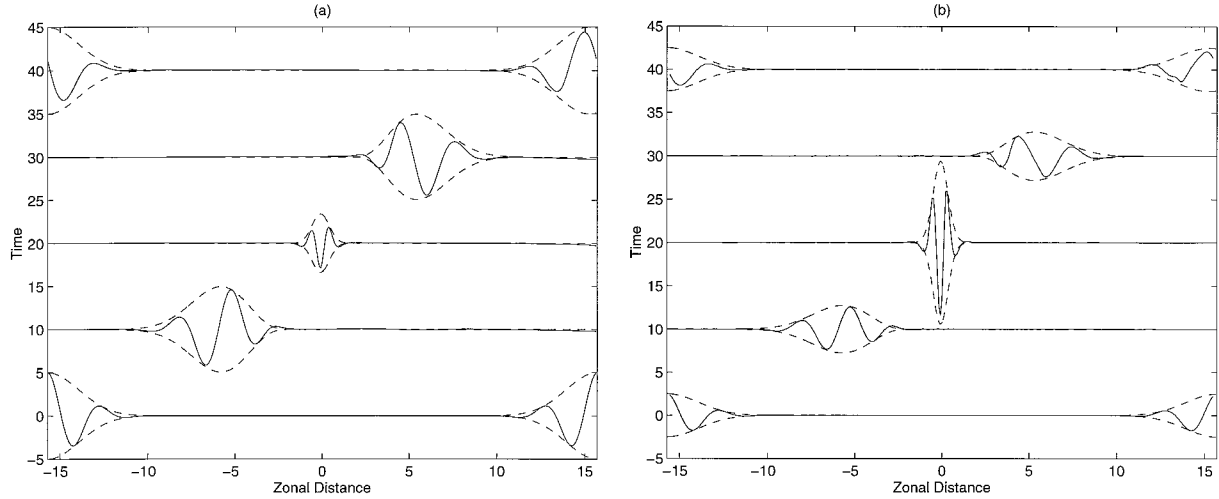


FIG. 15. Numerical simulation (solid) and WKB predictions (dashed) for wave propagation in the linear two-contour case example. (a) Perturbation streamfunction and (b) perturbation particle positions.

two-contour system, perhaps due to the coupling of symmetric and antisymmetric modes when the basic state is no longer slowly varying.

## 2) NONLINEAR CALCULATIONS

As in the one-contour model, it is expected that when the initial wave amplitude  $\eta_0$  is increased beyond a critical value, wave breaking will occur, leading to an irreversible loss of wave action and reduction in wave amplitude. Wave breaking in the two-contour model is interesting for two different reasons. First, since the shear (4.1) about each individual contour is not symmetric, we do not expect the breaking to be symmetric. Second, the two-contour model allows us to test the generality of the clipping hypothesis outlined in section 3b(2).

Similarly to section 3b(2), the calculation of the minimum particle displacement amplitude at which breaking occurs involves determining the wave amplitude for which a stagnation point in the total flow intersects the contour. For the two-contour model, it can be shown that this will occur for the critical particle displacement amplitude for breaking to occur,  $|\eta_{cr}|$ , satisfying

$$k|\eta_{cr}| \{2 - (1 + e^{-2k\gamma_0}) e^{-k|\eta_{cr}|}\} \approx 1 + e^{-2k\gamma_0}. \quad (4.15)$$

Comparing (3.23) and (4.15), we see that  $|\eta_{cr}|$  depends on the wavenumber  $k$ , as in the one-contour model, and additionally on the coupling parameter  $\gamma_0 k$ . In the strongly coupled limit  $\gamma_0 k \rightarrow 0$ , the breaking criterion is identical to the one-contour breaking criterion (3.24), namely  $k|\eta_{cr}| \approx 1.35$ . However, in the weakly coupled limit  $\gamma_0 k \rightarrow \infty$ , there is a quantitative change in the breaking criterion to  $k|\eta_{cr}| \approx 1.17$ . In other words, for a given wavenumber, waves break at smaller amplitudes

when the contours are far apart than they do when they are close together. This is primarily because the intrinsic phase velocity (the phase velocity relative to the basic flow on the contour) is smaller for widely separated contours, which follows from the dispersion relation (4.3).

To study breaking in the two-contour model, we use the same topographic forcing as in the one-contour simulations of section 3b(2) to generate a zonally varying mean flow. We use this topographic forcing because it facilitates direct comparison with the one-contour breaking results and because the strong zonal variations in the basic flow used to study linear wave propagation in section 4b(2) cause extensive breaking at small amplitudes that is computationally expensive to resolve. The basic-state along-contour velocity and particle positions are shown in Fig. 16; as in the one-contour model, the along-contour basic-state wind is reduced by a factor of 2 at the center of the domain. The initial condition for the numerical simulations below are particle displacements of the form (3.17) on each contour with  $k_0 = 2$  and  $x_0 = -5\pi$ , and integrations are performed for various values of  $\eta_0$  and  $\chi$ , similarly to section 3b(2).

Figure 17 provides an example of wave breaking in the two-contour model. The initial particle position amplitude for this simulation is  $\eta_0 = 0.2$ , with phase  $\chi = 0$ . Similarly to the one-contour model, the primary signature of wave breaking is the shedding of PV filaments. However, in the two-contour model breaking only occurs outward from each contour, provided the initial amplitude of the perturbation is sufficiently small. This agrees with the findings of Nakamura and Plumb (1994), who showed that waves typically break in the direction of stronger shear, which is outward in this case.

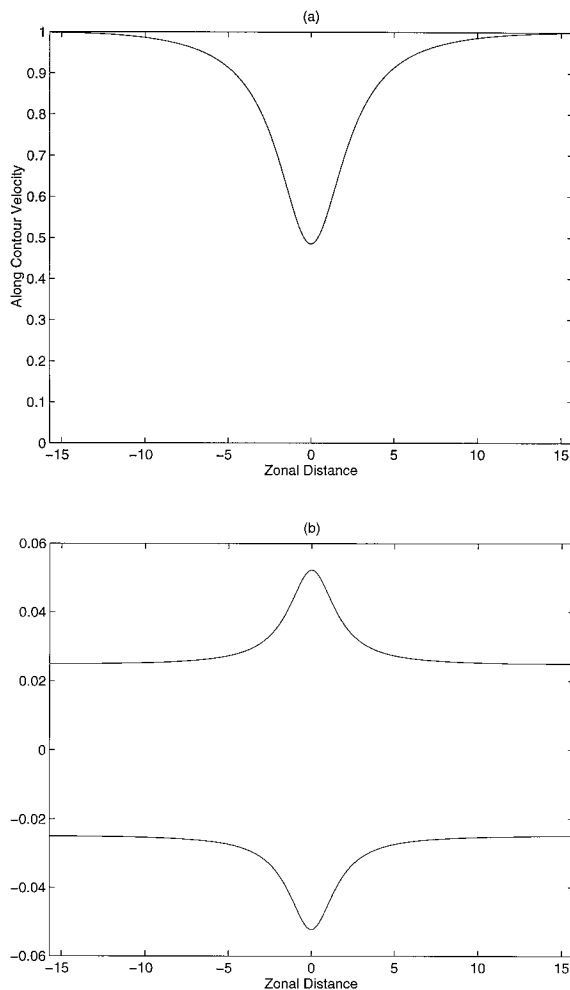


FIG. 16. (a) Basic-state along-contour velocity and (b) particle positions for nonlinear two-contour simulations.

As in the one-contour model, breaking results in the loss of wave action and the reduction of wave amplitude as it propagates through the weak flow region. Figure 18 summarizes the effects of breaking on the final wave amplitude for a series of experiments using the two-contour model and the topographic forcing of section 3b(2). The clipping hypothesis described in section 3b(2) for the one-contour model provides a reasonable description of the reduction in wave amplitude associated with breaking for the two-contour model. In particular, for this basic state and an initial value of  $k|_{x=-5\pi} = 2$ , (4.15) leads to the prediction that waves will break for  $|\eta_{cr}| > 0.298$  or  $\eta_0 \geq 0.15$ . The numerical results support this threshold, as no breaking is found for initial particle displacement amplitudes smaller than this value. The breaking experiments shown in Fig. 18 highlight two points in particular. First, even for cases which do not break, there is an approximately 10% reduction in wave amplitude upon passing through the weak flow region. Because this

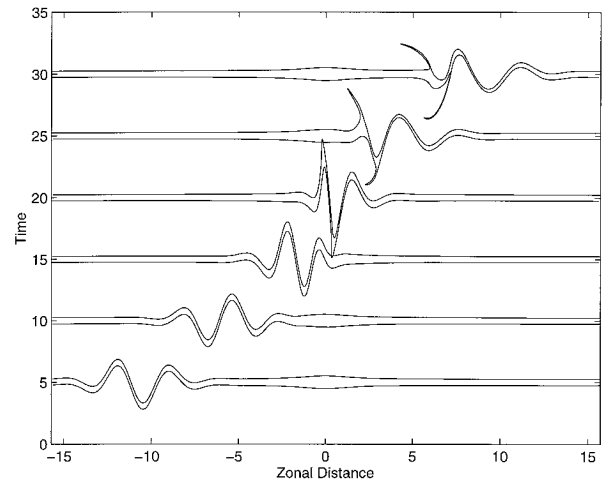


FIG. 17. Particle positions as a function of time for the two-contour simulation with initial perturbation amplitude  $\eta_0 = 0.4$  and phase  $\chi = 0$ .

reduction is significantly smaller in the wave action (not shown), it presumably results from the dispersion of the initially localized packet, as the group velocity for the two-contour symmetric modes is no longer wavenumber independent. Second, the amplitude reduction in waves that do break is even better described by the clipping-hypothesis (the solid curve in Fig. 18) than was the case for the one-contour simulations. There is significantly less spread of the wave amplitude about the clipping-hypothesis predicted value upon exiting the weak flow region.

## 5. Discussion

We have investigated the behavior of barotropic waves propagating through zonally varying contour distributions. In this simple framework, it is possible to make specific and testable predictions of eddy structural changes brought about by zonal variations in the basic flow. We have used conservation laws, WKB theory, and linear and nonlinear numerical simulations to determine the dependence of eddy wavelength, streamfunction amplitude, and Lagrangian particle displacement amplitude on zonally varying one- and two-contour storm track models. The one-contour model is relatively simple and instructive. The two-contour model adds realistic features appropriate for modeling upper-tropospheric eddies, by allowing eddies to be anisotropic and by allowing zonal variations in the effective PV gradient across the contours.

In the linear regime of small amplitude waves, the effect of zonal variability on eddy structure in the one- and two-contour models is similar. Because the one-contour model is linearly dispersive with  $\partial^2\omega/\partial^2k = 0$ , and the two-contour model has  $\partial^2\omega/\partial^2k$  small for  $\Delta y_0 \ll U_0$  [see (3.4) and (4.3)], the eddy wavelength scales with

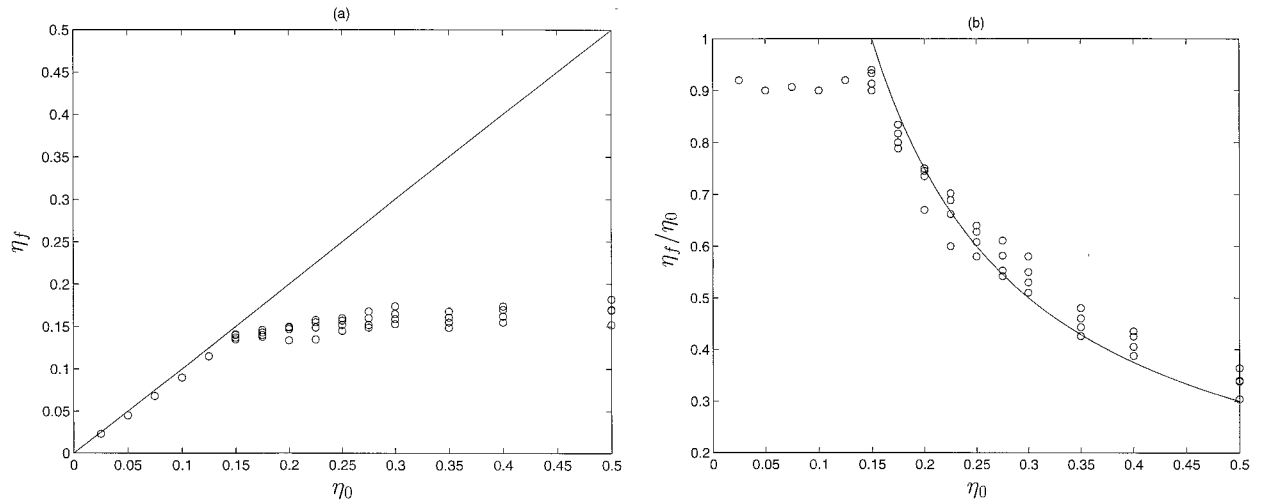


FIG. 18. As in Fig. 8 but for two-contour model simulations.

the along-contour velocity in both models. In a weak flow region, for example, the eddy wavelength shortens to maintain the same packet frequency. Conservation of wave action (or pseudoenergy) then leads to the prediction that eddy streamfunction amplitude remains constant in the one-contour model and is weakly modulated in the two-contour model. Lagrangian particle displacement amplitude, on the other hand, scales inversely with the along-contour flow; in a weak flow region it is greatly amplified.

In the nonlinear regime of finite-amplitude waves, the models still share important features. Wave breaking is greatly enhanced in weak flow regions since stagnation points approach the basic-state contour most closely and since the contour displacements are largest in these regions. In both models, this breaking is characterized (i) by filamentation rather than vortex roll-up; (ii) by reduction, or “clipping” of the contour displacement amplitude to the minimum distance between the stagnation points and the basic-state contour; (iii) by a significant loss of the wave action associated with the packet; (iv) by an increase of the disturbance wavelength; and (v) by an associated reduction of the disturbance frequency.

Despite the similarities in the nature of the breaking, the meridional distribution of the breaking is quite different in the two models. In the one-contour model, the symmetry of the basic flow shear implies that the breaking and clipping are symmetric about the contour. In the two-contour model, by contrast, the asymmetry in the basic flow shear implies that breaking and clipping occur preferentially toward the region of stronger shear, which is toward the exterior of the contours in the case examined in section 4b.

The result, from the linear theory in sections 3a and 4a, that the streamfunction amplitude is at most only weakly modulated by the underlying basic flow in these

models, differs from the results of Lee (1995). Lee studied barotropic  $f$ -plane eddy dynamics in the absence of basic-state PV gradients and found that the rms eddy streamfunction scales as the square of the zonal flow, that is,  $\langle \psi^2 \rangle^{1/2} \sim U^2$ . Because Lee focused on eddies with little meridional structure, a more appropriate field to compare to Lee’s results might be the meridionally integrated contour disturbance streamfunction, which scales as  $\langle \psi^2 |_{\text{contour}} \rangle^{1/2} / k \propto U$  in our contour models. This quantity indicates some local weakening of streamfunction variance in regions of weak flow, but the dependence on  $U$  is weaker than in Lee’s analysis.

Understanding the dependence of upper-tropospheric eddy amplitudes on the local zonal flow is important in developing a theory of the longitudinal structure of the storm tracks. For example, Lee (1995), based on the prediction that  $\langle \psi^2 \rangle^{1/2} \propto U^2$ , suggested that “barotropic modulation” of eddies could be in part responsible for the observed storm track eddy amplitude modulations and, in particular, for the termination of the storm tracks at the jet exit regions. The results presented here, if meridionally integrated streamfunction variance is used as the measure of eddy activity, support this suggestion, albeit with a weaker dependence on variations in the zonal flow. Nonlinearities are presumably important in the observed reduction in eddy activity as well. The nonlinear CS simulations presented in sections 3b(2) and 4b lead to the picture that nonlinearities associated with wave breaking and filamentation in the weak flow region result in a decrease in the barotropic eddy activity in excess of that expected from purely linear modulation. This reduction depends strongly on the measure of eddy variance, however. Wave action, since it is conserved by the dynamics, can only be lost if wave breaking takes place. However, other measures of eddy activity are

ambiguous and may increase or decrease reversibly depending on the structural changes brought about by the mean flow modulation and wave breaking.

Regarding directions of further study, the reduction in frequency due to nonlinear breaking investigated in section 3 indicates that, at least for simple contour models like these, nonlinear effects and scale interactions can lead to the generation of low-frequency variability. The possibility of such a mechanism existing in the atmosphere is intriguing, as it is a mechanism with no linear manifestation, but it could potentially be important given the strong deformation of PV contours and wave breaking associated with the termination of the storm tracks. The dynamical basis for this mechanism needs to be better understood and its possible existence in more complicated models and in the observations further explored.

Finally, the inclusion of baroclinic effects represents a significant step in difficulty above the analysis presented above. Exponentially growing modes have zero vertically integrated wave action, and hence it is not apparent a priori how to apply wave action conservation. However, as wave action is typically sign-definite in the upper troposphere, a heuristic wave action equation for the upper troposphere of the form

$$\frac{\partial \mathcal{W}}{\partial T} = -\frac{\partial}{\partial X}(c_g \mathcal{W}) - \text{clipping} + \text{baroclinic source} \tag{5.1}$$

can be hypothesized. Application of such a simple equation diagnostically to model baroclinic storm tracks will hopefully lead to new insights regarding the relative roles of barotropic and baroclinic processes in generating the modulations in eddy variance. Understanding how the baroclinic source term is related to the upper-level wave action even in simple models would be a significant step in the development of a complete theory of tropospheric storm tracks.

*Acknowledgments.* The authors would like to thank Steve Garner and Isidoro Orlanski for reviewing the manuscript. Discussions with Alan Plumb were particularly useful, and we gratefully acknowledge his observation that it is the stagnation point in the total flow, rather than simply the linear theory critical line for the basic flow, that determines the wave breaking criteria used in sections 3b(2) and 4b(2). Additionally, we acknowledge Moto Nakamura for helpful discussions. KLS and PJK were supported by NOAA Grant NA67RJ0120, and PJK acknowledges support from a Natural Sciences and Engineering Research Council/Canada fellowship. The views expressed herein do not necessarily represent those held by NOAA or any of its subagencies.

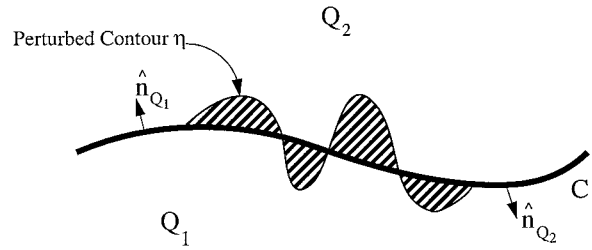


FIG. 19. Region in which generalized enstrophy contribution to pseudoenergy is nonzero.

APPENDIX A

Derivation of Eqs. (2.6) and (2.7)

The tangential–normal coordinates ( $s, n$ ) described in section 2a satisfy

$$\partial_{xy}(s, n) = 1 \text{ and } |\nabla n| = |\nabla s| = 1. \tag{A.1}$$

The transformation is a local rotation of coordinates and is therefore area and orientation preserving.<sup>1</sup>

The component of the velocity tangential to the contour is

$$\dot{s} = \nabla s \cdot (-(\Psi + \psi)_{,s}(\Psi + \psi)_{,x}) = -(\Psi + \psi)_{,n}, \tag{A.2}$$

and similarly the component of the velocity normal to the contour is

$$\dot{n} = (\Psi + \psi)_{,s}. \tag{A.3}$$

From (A.2)–(A.3), the basic-state velocity is  $\mathbf{U} = (-\partial_n \Psi, \partial_s \Psi)$  and the perturbation velocity is  $\mathbf{u} = (-\partial_n \psi, \partial_s \psi)$ .

Consider now the linearized dynamics. Near contour  $j$ ,  $\partial_s Q = 0$ , and using (A.1), (2.3) becomes

$$\frac{\partial q}{\partial t} + \partial_{sn}(\Psi, q) + \Delta_j \delta(n) \partial_s \psi = 0, \text{ near contour } j, \tag{A.4}$$

where  $\delta(\cdot)$  is the Dirac delta distribution. Then we may obtain (2.6) by transforming  $\nabla^2$  to ( $s, n$ ) coordinates and integrating across the contour and using the fact that  $\partial_s \Psi$  vanishes along the contour.

We obtain (2.7) as follows. The small-amplitude Lagrangian displacement,  $\xi = (\xi, \eta)$ , satisfies (e.g., Drazin and Reid 1981, section 15.1)

$$\mathbf{u} = \frac{\partial \xi}{\partial t} + \mathbf{U} \cdot \nabla \xi - \xi \cdot \nabla \mathbf{U}. \tag{A.5}$$

<sup>1</sup> Demonstration of (A.1): For an arbitrary function  $g$  we have

$$\frac{\partial g}{\partial n} = \frac{\partial x}{\partial n} \frac{\partial g}{\partial x} + \frac{\partial y}{\partial n} \frac{\partial g}{\partial y} = \nabla g \cdot \mathbf{n} = \hat{n}_{(\omega)} \frac{\partial g}{\partial x} + \hat{n}_{(\omega)} \frac{\partial g}{\partial y},$$

where the notation  $\hat{n}_{(\omega)}$ , for example, denotes the  $x$  component of  $\mathbf{n}$ . This, together with an analogous statement for  $\partial_s g$ , and using the fact that  $\hat{\mathbf{s}} = \mathbf{n} \times \hat{\mathbf{z}}$ , implies (A.1).

Using the above definitions of  $\mathbf{U}$  and  $\mathbf{u}'$  the  $n$  component of (A.5) is

$$\partial_s \psi_j = \frac{\partial \eta_j}{\partial t} + \frac{\partial(U_j \eta_j)}{\partial s}. \tag{A.6}$$

Comparing (A.6) and (2.6), (2.7) immediately follows apart from a constant of integration that may be set to zero.

APPENDIX B

**Pseudoenergy Conservation**

We divide the full domain  $\Omega$  into a disturbance region,  $\Omega_q$ , where  $q$  is nonzero, and its complementary region,  $\Omega_Q = \Omega \setminus \Omega_q$ , where  $q = 0$  but where  $\psi$  may be nonzero. The region  $\Omega_q$  is represented by the hatching in Fig. 19.

The local flux law for pseudoenergy is (McIntyre and Shepherd 1987)

$$\partial_t \mathcal{A} + \nabla \cdot \mathbf{J} = 0, \tag{B.1}$$

where the pseudoenergy density is

$$A = E + B = \frac{1}{2} |\nabla \psi|^2 + \int_0^q \{\Psi(Q + \tilde{q}) - \Psi(Q)\} d\tilde{q} \tag{B.2}$$

and the pseudoenergy flux is

$$\mathbf{J} = (B - q\psi)(\mathbf{U} + \mathbf{u}) - \psi \nabla(\partial_t \psi) + (\frac{1}{2}) \psi^2 \mathbf{z} \times \nabla Q, \tag{B.3}$$

where  $\mathbf{U}$  is the basic-state velocity and  $\mathbf{u}$  is the disturbance velocity. Using the boundary conditions described in section 2, we have

$$\frac{d\mathcal{A}}{dt} = \int_{\Omega} A dx dy = 0. \tag{B.4}$$

The pseudoenergy  $\mathcal{A}$  may be expressed in terms of quantities local to the contours. In  $\Omega_Q$ ,  $q = 0$ , implying that  $B = 0$  and

$$A = E = \frac{1}{2} |\nabla \psi|^2 = \nabla^2 \left( \frac{1}{4} \psi^2 \right). \tag{B.5}$$

Then

$$\int_{\Omega_Q} A dx dy = \sum_{j=1}^{N+1} \int_{\Omega_{Q_j}} A dx dy = \sum_{j=1}^{N+1} \oint_{\partial \Omega_{Q_j}} \nabla \left( \frac{1}{4} \psi^2 \right) \cdot \mathbf{n}_{Q_j} ds, \tag{B.6}$$

where  $\Omega_{Q_j}$  represents part of  $\Omega_Q$  with  $Q = Q_j$ ,  $\partial \Omega_{Q_j}$  represents the boundary of  $\Omega_{Q_j}$ , and  $\mathbf{n}_{Q_j}$  represents the outward normal to that region. Equation (B.6) may also be interpreted as the flux of  $\nabla(\frac{1}{4}\psi^2)$  into the disturbance region  $\Omega_{Q_j}$  associated with contour  $j$ ; that is,

$$\int_{\Omega_Q} A dx dy = - \sum_{j=1}^N \oint_{\partial \Omega_{Q_j}} \nabla \left( \frac{1}{4} \psi^2 \right) \cdot \mathbf{n}_{Q_j} ds, \tag{B.7}$$

where  $\mathbf{n}_{Q_j} = -\mathbf{n}_{Q_j}$ . For small-amplitude disturbances, then

$$\int_{\Omega_Q} A dx dy \approx \sum_{j=1}^N \int_{y_j} - \left[ \nabla \left( \frac{1}{4} \psi^2 \right) \cdot \mathbf{n}_j \right] ds, \tag{B.8}$$

where  $\mathbf{n}_j$  is the unit normal to the  $j$ th contour and points to the left of direction of increasing arc length  $s$ , and the notation  $[[\cdot]]_j$  indicates a jump in the value of the quantity  $(\cdot)$  across a contour. However, from (2.7), it follows that  $\nabla \psi \cdot \mathbf{n}_j = -\Delta_j \eta_j$ , and this expression simplifies to

$$\int_{\Omega_Q} A dx dy \approx \sum_{j=1}^N \int_{y_j} \frac{1}{2} \Delta_j \psi_j \eta_j ds, \tag{B.9}$$

where  $\psi_j = \psi(s, 0)$  is the disturbance streamfunction evaluated along contour  $j$ .

In  $\Omega_q$ ,  $B$  is evaluated following the method described in Shepherd (1988, appendix B) for expressing the pseudomomentum defined with respect to piecewise constant zonal PV distributions. Within  $\Omega_q$ , assuming that the disturbed contour  $j$  does not cross the location of another basic-state contour,

$$B(s, n) = \text{sgn}(n) \Delta_j \{\Psi(s, n) - \Psi_j\} = -U_j \Delta_j |n| + O(\Delta_j \nabla^2 \Psi n^2), \tag{B.10}$$

where  $\Psi_j = \Psi(s, 0)$  is the value of  $\Psi$  on the contour  $j$ ,  $U_j = -\nabla \Psi \cdot \mathbf{n}$  is the basic-state velocity component tangential to the contour, and  $n$  is the displacement normal to the basic-state contour. Letting  $\eta_j$  represent the disturbed contour's displacement, then  $B \sim -U_j \Delta_j \eta_j$  is linear in the disturbance amplitude, but  $E$  is quadratic and therefore comparatively small for small-amplitude disturbances. Therefore,

$$\begin{aligned} \int_{\Omega_q} A dx dy &= \sum_{j=1}^N \int_{\Omega_{q_j}} A dx dy \\ &= \sum_{j=1}^N \int_{y_j} \int_0^{\eta_j} (\text{sgn}(\hat{n}) \Delta_j \{\Psi(s, \hat{n}) - \Psi(s, 0)\} + E) d\hat{n} ds \end{aligned} \tag{B.11}$$

$$\approx \sum_{j=1}^N \int_{y_j} - \frac{1}{2} U_j \Delta_j \eta_j^2 ds. \tag{B.12}$$

In (B.11), the change of variables from Cartesian coordinates  $(x, y)$  makes use of (A.1).

Combining (B.4), (B.7), and (B.11) yields a finite-amplitude conservation law for the wave activity associated with contour perturbations. For small-amplitude disturbances, from (B.9) and (B.12), the conserved pseudoenergy is given by (2.8) with (2.10).

## APPENDIX C

**WKB Solution for the One-Contour Model**

In order to construct a WKB solution to the one-contour problem with a zonally varying basic flow, we note that solutions of the form

$$\psi^\pm = \psi(X \pm iY) \quad (\text{C.1})$$

exactly satisfy Laplace's equation away from the contour, where

$$(X, Y) = \epsilon(x, y). \quad (\text{C.2})$$

The form of this solution implies that if the streamfunction is oscillatory in the zonal direction, it is evanescent in the meridional direction. Assuming a WKB-type solution of the form

$$\psi^\pm = \Phi^\pm e^{iS^\pm/\epsilon} + \text{complex conjugate}, \quad (\text{C.3})$$

it follows that

$$\begin{aligned} \partial_x \psi^\pm &= (iS^{\pm'} \Phi^\pm + \epsilon \Phi^{\pm'}) e^{iS^\pm/\epsilon}, \\ \partial_y \psi^\pm &= \pm i(iS^{\pm'} \Phi^\pm + \epsilon \Phi^{\pm'}) e^{iS^\pm/\epsilon}, \\ \partial_{xy}^2 \psi^\pm &= \pm i(-S^{\pm'2} \Phi^\pm + i\epsilon(2S^{\pm'} \Phi^{\pm'} + S^{\pm''} \Phi^\pm) \\ &\quad + \epsilon^2 \Phi^{\pm''}) e^{iS^\pm/\epsilon}, \end{aligned} \quad (\text{C.4})$$

where the prime denotes differentiation with respect to the argument. For the one-contour case, we seek solutions of the form

$$\psi = \tilde{\psi} e^{-i\omega t} + \text{complex conjugate} \quad (\text{C.5})$$

and the spatial dependence

$$\tilde{\psi} = \begin{cases} \Phi^+ e^{iS^+/\epsilon} & \text{for } y > 0 \\ \Phi^- e^{iS^-/\epsilon} & \text{for } y < 0. \end{cases} \quad (\text{C.6})$$

The appropriate solution branches have been chosen in the above to satisfy the boundary condition that  $\tilde{\psi} \rightarrow 0$  as  $|y| \rightarrow \infty$  as well as to ensure the continuity of the solution at  $y = 0$ , where  $S^+ = S^- = S$  and  $\Phi^+ = \Phi^- = \Phi$ .

Defining  $k \equiv S'$ , at  $y = 0$ , we have to order  $\epsilon$

$$\partial_x \tilde{\psi} = (ik\Phi + \epsilon\Phi') e^{iS/\epsilon}, \quad (\text{C.7})$$

$$[\partial_y \tilde{\psi}]_{y=0} = 2i(ik\Phi + \epsilon\Phi') e^{iS/\epsilon}, \quad (\text{C.8})$$

$$[\partial_{xy}^2 \tilde{\psi}]_{y=0} = 2i(-k^2\Phi + i\epsilon(2k\Phi' + k'\Phi)) e^{iS/\epsilon}. \quad (\text{C.9})$$

Substituting these expressions into the equation of motion (3.2), we find to order  $\epsilon$

$$\begin{aligned} 2\omega(ik\Phi + \epsilon\Phi') + 2iU_0(-k^2\Phi + i\epsilon(2k\Phi' + k'\Phi)) \\ - \epsilon 2U_0' k\Phi + \Delta(ik\Phi + \epsilon\Phi') = 0. \end{aligned} \quad (\text{C.10})$$

The leading-order terms yield the dispersion relation,

$$\omega = U_0 k - \Delta/2, \quad (\text{C.11})$$

as expected from (3.4).

At order  $\epsilon$ , an equation for the streamfunction amplitude at  $y = 0$  is obtained, namely

$$(U_0 k \Phi)' = 0. \quad (\text{C.12})$$

Using the dispersion relation (C.11), we have  $U_0 k = \omega + \frac{1}{2}\Delta = \text{constant}$ , implying that

$$\Phi = \text{const}, \quad (\text{C.13})$$

that is, that the streamfunction amplitude  $|\psi|$  is conserved as the eddies propagate through the zonally varying flow.

## REFERENCES

- Andrews, D. G., and M. E. McIntyre, 1978: An exact theory of nonlinear waves on a Lagrangian-mean flow. *J. Fluid Mech.*, **89**, 609–646.
- Arnol'd, V. I., 1966: On an a priori estimate in the theory of hydrodynamical stability (in Russian). *Izv. Vyssh. Uchebn. Zaved. Matematika*, **54**, 3–5.
- Bretherton, F. P., and C. J. R. Garrett, 1968: Wave trains in inhomogeneous moving media. *Proc. Roy. Soc. London, Ser. A*, **302**, 529–554.
- Dickinson, R. E., 1968: Planetary Rossby waves propagating vertically through weak westerly wind waveguides. *J. Atmos. Sci.*, **25**, 984–1002.
- Dole, R. M., 1986: Persistent anomalies of the extratropical Northern Hemisphere wintertime circulation: Structure. *Mon. Wea. Rev.*, **114**, 178–207.
- Drazin, P. G., and W. H. Reid, 1981: *Hydrodynamic Stability*. Cambridge University Press, 527 pp.
- Dritschel, D. G., 1988: Contour surgery: A topological reconnection scheme for extended integrations using contour dynamics. *J. Comput. Phys.*, **77**, 240–266.
- , 1989a: Contour dynamics and contour surgery: Numerical algorithms for extended, high-resolution modeling of vortex dynamics in two-dimensional, inviscid, incompressible flows. *Comput. Phys. Rep.*, **10**, 77–146.
- , 1989b: On the stabilization of a two-dimensional vortex strip by adverse shear. *J. Fluid Mech.*, **206**, 193–221.
- Grimshaw, R., 1984: Wave action and wave-mean flow interaction, with application to stratified shear flows. *Annu. Rev. Fluid Mech.*, **16**, 11–44.
- Hoskins, B. J., and P. J. Valdes, 1990: On the existence of storm-tracks. *J. Atmos. Sci.*, **47**, 1854–1864.
- , and T. Ambrizzi, 1993: Rossby wave propagation on a realistic longitudinally varying flow. *J. Atmos. Sci.*, **50**, 1661–1671.
- , M. E. McIntyre, and A. W. Robertson, 1985: On the use and significance of isentropic potential vorticity maps. *Quart. J. Roy. Meteor. Soc.*, **111**, 877–946.
- Killworth, P. D., and M. E. McIntyre, 1985: Do Rossby-wave critical layers absorb, reflect, or over-reflect? *J. Fluid Mech.*, **161**, 449–492.
- Lau, N.-C., 1988: Variability of the observed midlatitude storm tracks in relation to low-frequency changes in the circulation pattern. *J. Atmos. Sci.*, **45**, 2718–2743.
- Lee, S., 1995: Localized storm tracks in the absence of local instability. *J. Atmos. Sci.*, **52**, 977–989.
- McIntyre, M. E., and T. G. Shepherd, 1987: An exact local conservation theorem for finite-amplitude disturbances to non-parallel shear flows, with remarks on Hamiltonian structure and on Arnol'd's stability theorems. *J. Fluid Mech.*, **181**, 527–565.
- Mullen, S. L., 1987: Transient eddy forcing of blocking flows. *J. Atmos. Sci.*, **44**, 3–22.
- Nakamura, H., and J. M. Wallace, 1993: Synoptic behavior of baroclinic eddies during the blocking onset. *Mon. Wea. Rev.*, **121**, 1892–1903.
- Nakamura, M., and R. A. Plumb, 1994: The effects of flow asymmetry

- on the direction of Rossby wave breaking. *J. Atmos. Sci.*, **51**, 2031–2045.
- Pedlosky, J., 1987: *Geophysical Fluid Dynamics*. 2d ed. Springer-Verlag, 710 pp.
- Pierrehumbert, R. T., 1980: A family of steady, translating vortex pairs with distributed vorticity. *J. Fluid Mech.*, **99**, 129–144.
- Pieters, D., and W. D. Waugh, 1996: Influence of barotropic shear on the poleward advection of upper-tropospheric air. *J. Atmos. Sci.*, **53**, 3013–3031.
- Polvani, L. M., and R. A. Plumb, 1992: Rossby wave breaking, filamentation, and secondary vortex formation: The dynamics of a perturbed vortex. *J. Atmos. Sci.*, **49**, 462–476.
- , G. R. Flierl, and N. J. Zabusky, 1989: Filamentation of unstable vortex structures via separatrix crossing: A quantitative estimate of onset time. *Phys. Fluids A*, **1**, 181–184.
- Shepherd, T. G., 1988: Rigorous bounds on the nonlinear saturation of instabilities to parallel shear flows. *J. Fluid Mech.*, **196**, 291–322.
- Wallace, J. M., and M. L. Blackmon, 1983: Observations of low-frequency atmospheric variability. *Large Scale Dynamical Processes in the Atmosphere*, B. J. Hoskins and R. Pearce, Eds., Academic Press, 55–94.
- Warn, T., and Warn, H., 1978: Evolution of a nonlinear critical level. *Stud. Appl. Math.*, **59**, 37–71.
- Waugh, D. W., L. M. Polvani, and R. A. Plumb, 1994: Nonlinear, barotropic response to a localized topographic forcing: Formation of a “tropical surf zone” and its effect on interhemispheric propagation. *J. Atmos. Sci.*, **51**, 1401–1416.
- Whitham, G. B., 1965: A general approach to linear and non-linear dispersive waves using a Lagrangian. *J. Fluid Mech.*, **22**, 273–283.